UNIVERSITÀ
DI PAVIA

Dipartimento di Biologia e Biotecnologie “L. Spallanzani”

Laurea Magistralis in Neurobiology

Effects of the Synthetic Cannabinoid JWH-018 on the Central Nervous System: a Morphological and Immunohistochemical Study in Mice.

Supervisor:
Prof. Fabrizio De Luca

Co-supervisors:
Prof.ssa Elisa Roda
Dott.ssa Emma Lugli

Experimental thesis by
Nicolò Di Bella

Academic Year 2025/2026

Thesis title

ENG Effects of the Synthetic Cannabinoid JWH-018 on the Central Nervous System: a Morphological and Immunohistochemical Study in Mice

ITA Effetti del cannabinoide sintetico JWH-018 sul Sistema Nervoso Centrale: uno studio Morfologico e Immunoistochimico su topi.

ABSTRACT

ITA: Negli ultimi anni, la diffusione delle Nuove Sostanze Psicoattive (NPS) ha delineato una crescente ed allarmante emergenza sanitaria e tossicologica. All'interno di questo eterogeneo panorama, i cannabinoidi sintetici rappresentano una delle classi più diffuse e insidiose, caratterizzati da un'elevata affinità e potenza agonista verso i recettori cannabinoidi rispetto al fitocannabinoide Δ^9-THC, con conseguenti profili di tossicità acuta e cronica ancora parzialmente inesplorati.

Il presente lavoro di tesi si propone di valutare gli effetti neurotossici indotti dall'esposizione al cannabinoide sintetico JWH-018 a livello del sistema nervoso centrale (SNC) in un modello murino. Nello specifico, l'indagine si è focalizzata sull'analisi morfologica e immunoistochimica di tre regioni chiave costituenti il *core* del controllo motorio: la corteccia motoria primaria, il caudato-putamen e il cervelletto. Al fine di indagare se l'alterazione dell'omeostasi del calcio cellulare costituisca un meccanismo biologico sottostante alla neurotossicità, è stata condotta un'analisi immunoistochimica quantitativa e semiquantitativa mirata all'espressione delle tre principali proteine leganti il calcio: parvalbumina, calbindina e calretinina. Le indagini morfologiche hanno evidenziato una compromissione dell'integrità strutturale del parenchima nelle diverse aree esaminate, caratterizzata da vacuolizzazione del neuropilo, apprezzabile sotto forma di aree bianche vuote, associata alla presenza di foci microemorragici, particolarmente evidenti a livello della citoarchitettura cerebellare. Parallelamente, l'analisi immunoistochimica ha rivelato un decremento della densità ottica (OD) per le proteine leganti il calcio a livello delle aree cerebrali indagate, unitamente a un peculiare andamento layer-specific nella corteccia cerebellare. Questo quadro suggerisce un possibile fenomeno di exhaustion dei sistemi di buffering del calcio intracellulare, secondario a un sovraccarico ionico e allo stress cellulare indotto da JWH-018. Nel loro insieme, tali riscontri riflettono neurotossicità mediata dai cannabinoidi sintetici nei circuiti motori, individuando nella disregolazione dell'omeostasi del calcio e nel conseguente danno parenchimale e vascolare un nodo centrale.

INDICE

1 INTRODUCTION 1

1.1 New Psychoactive Substances 1

1.2 Synthetic Cannabinoids 4

1.3 JWH-018 7

1.4 The Endocannabinoid System 9

1.4.1 *Cannabinoid receptors* 11

1.5 Calcium Ions And The Central Nervous System 14

1.5.1 *Role of calcium in the central nervous system* 14

1.5.2 *Calcium homeostasis in neurons* 15

1.5.3 *Effects of synthetic cannabinoids on intracellular calcium levels* 17

2 CENTRAL NERVOUS SYSTEM: CEREBRAL CORTEX, DORSAL STRIATUM AND CEREBELLUM 19

2.1 Gross Morphology And Cellular Organization Of The Cerebral Cortex 21

2.1.1 *Motor cortex* 24

2.2 Caudate Nucleus And The Putamen: Gross Morphology And Cellular Organization .. 25

2.2.1 *Microscopical organization* 26

2.2.2 *Caudate Putamen circuitry* 27

2.3 The Cerebellum 28

2.3.1 *Anatomy of the cerebellum* 28

2.3.2 *Cerebellar cortex* 31

2.3.3 *Cerebellar neural circuits* 34

2.3.4 *Higher cognitive and motor functions of the cerebellum* 35

3 AIM OF THE STUDY 37

4 MATERIAL AND METHODS 38

4.1 Animals 38

4.2 Drug Preparation And Doses Choice 38

4.3 Experimental Design 39
4.4 Tissue Preparation 39
4.5 Hematoxylin And Eosin 39
4.6 Immunohistochemical Reactions 40
4.7 Quantitative Analysis: Optical Density 41
4.8 Statistical Analysis 42
5 RESULTS 43
5.1 Gross Morphology 43
5.2 Immunohistochemistry 44
6 DISCUSSION 51
7 CONCLUSIONS 60
8 BIBLIOGRAPHY 61

1 INTRODUCTION

1.1 New Psychoactive Substances

New Psychoactive Substances (NPS) are defined as ' new narcotic or psychotropic drugs, in pure form or in preparation, that are not controlled by the United Nations drug conventions, but which may pose a public health threat comparable to that posed by substances listed in these conventions' (EMCDDA, 2005). Generally, these substances are synthesized as structural analogs or derivatives of compounds with well-established biological mechanisms, specifically to mimic their effects. NPS are designed with chemical structures slightly modified from those of controlled drugs and illicit substances to circumvent existing legislation, this allows the legal commercialization of compounds that mimic the effects of conventional drugs, which are consequently referred to as 'legal highs'. The problem is compounded by the common misconception that these products are safe and legal alternatives to classic drugs. This lack of regulatory control poses a direct risk to human health (A. Shafi et al., 2020). NPS share common administration routes with conventional illicit drugs, including oral ingestion, nasal insufflation, inhalation, and injection. The category of NPS comprises a chemically diverse group of compounds categorized by structural class and clinical toxicity (Fig. 1). Synthetic and semi-synthetic cannabinoids mimic Δ^9-THC by targeting endocannabinoid receptors; their high potency often elicits anxiety, hallucinations, seizures, and fatal intoxications. Synthetic cathinones (β-keto phenethylamines) and phenethylamines (such as 2C series and NBOMe drugs) alter central monoaminergic transmission, triggering agitation, insomnia, severe hyperthermia, seizures, hypertension, and fatalities. Similarly, aminoindanes produce stimulant and euphoric effects via Central Nervous System (CNS) monoamine modulation and can cause panic attacks, tachycardia, and lethal toxicity, while piperazines mimic MDMA-like actions, frequently resulting in hyperthermia, life-threatening serotonin syndrome, rhabdomyolysis, and death; Synthetic opioids, including fentanyl analogues, tramadol, and methadone, represent an acute overdose hazard driven by CNS opioid receptor activation that precipitates miosis, coma, and lethal respiratory depression. Tryptamines, such as psilocybin and DMT, share structural homology with 5-HT and cause profound perceptual alterations accompanied by mydriasis, catalepsy, cardiovascular complications, and fatalities. In parallel, dissociative drugs (e.g., ketamine, PCP, dextromethorphan) act as NMDA receptor antagonists, inducing marked disruptions in consciousness, amnesia, psychomotor agitation, nystagmus, and neurotoxicity. Lastly, plant-based NPS encompass traditional botanicals, including Catha edulis (khat), Mitragyna speciosa (kratom), and Salvia divinorum, as well as ayahuasca and kava, whose active alkaloids present substantial risks

of addiction, paranoia, motor incoordination, cardiovascular events, and respiratory failure. They are sold in various physical forms: synthetic cathinones are typically available as powders, tablets, or liquids, while synthetic cannabinoids are applied to plant materials to mimic natural products. Furthermore, the use of NPS is not limited to any specific group but spans age groups, socioeconomic backgrounds, and geographic areas (A. Y. Simão et al., 2022). The absence of standardized production and quality control makes it difficult to evaluate the pharmacological effects and clinical risks of NPS. Users can experience severe adverse effects, such as acute psychosis, epileptic seizures, and fatal toxicity. Consequently, regulatory frameworks must be flexible and responsive to keep pace with the evolving NPS market and reduce public health risks (M. Asan et al., 2023). The expanding technical capacity of the pharmaceutical sector has accelerated the arrival of novel psychoactive substances on the illicit market. Recent epidemiological and seizure data highlight the scale of this issue: in 2021, EU Member States seized a record 8. 5 tons of NPS (approximately 400 different substances) (EMCDDA, 2023); in 2022, the European Monitoring Centre for Drugs Addiction (EMCDDA) tracked around 930 NPS, including 41 newly identified compounds; past- year use among 15- to 34- year- olds (excluding GHB and ketamine) varied widely by country, from 0. 1% in Latvia to 5. 1% in Romania (EMCDDA, 2023); data from 2019 among 15- to 16- year- old students showed lifetime NPS use ranging from 0.9% to 6.6%, driven mainly by synthetic cannabinoids (1.1%-5.2%) and synthetic cathinones (0.2%–2.5%) (EMCDDA, 2023).

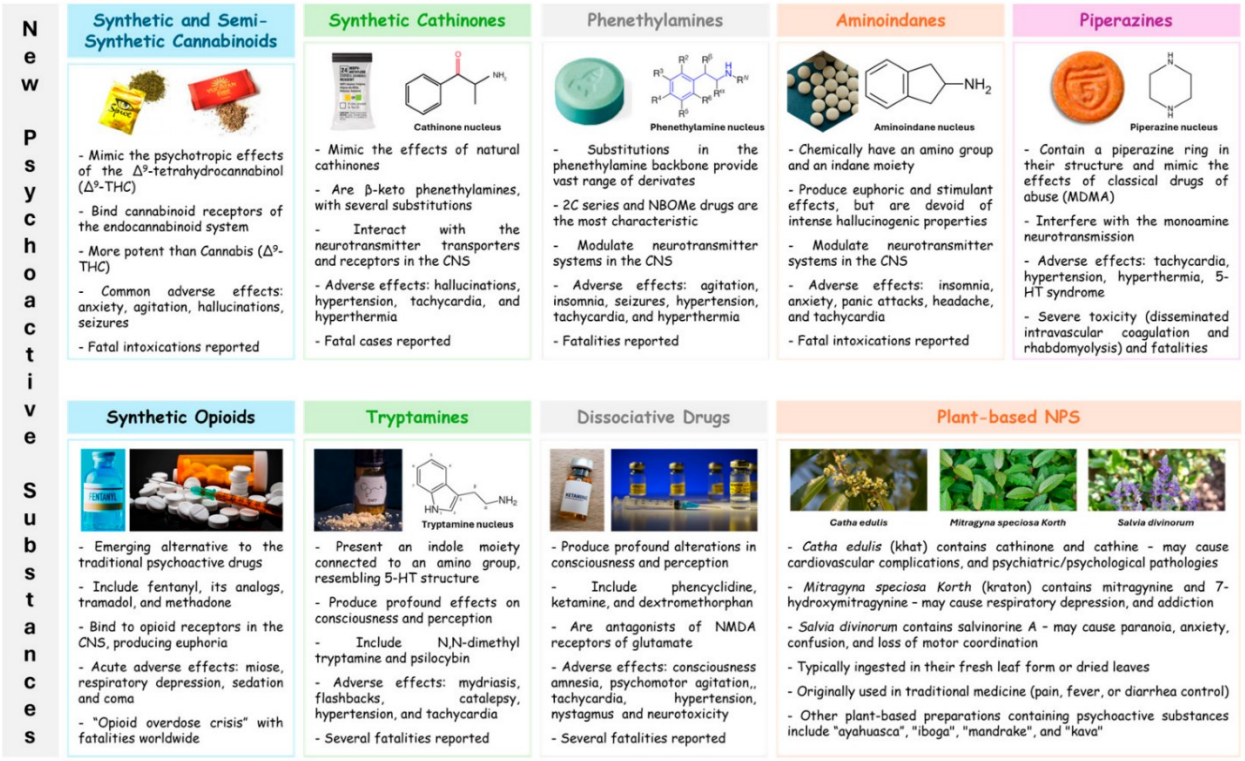


Figure 1. Summary diagram of the main types of NPS (image adapted from Ines C. Santos et al., 2024).

Addressing the challenges of NPS requires an integrated, dynamic approach combining scientific research, legislative action, and public health initiatives. Given the expanding chemical diversity of these substances, continuous monitoring and investigation are essential.

1.2 Synthetic Cannabinoids

First synthesized in the 1970s as research tools to study the endocannabinoid system, synthetic cannabinoids (SCs) have shifted toward the recreational "legal highs" market since 2000, serving as alternatives to plant-derived phytocannabinoids. Marketed as herbal blends and publicly known as "Spice", these drugs have gained popularity over the past decade as legal cannabis alternatives, particularly among adolescents, unhoused populations and incarcerated individuals (Joseph et al., 2017). Scientifically classified as Synthetic Cannabinoid Receptor Agonists (SCRAs), this group of NPS shares a binding affinity for the same cannabinoid receptors as natural phytocannabinoids (May et al., 2019). The widespread familiarity with cannabis established a receptive consumer base, while the ability of SCs to escape standard THC drug screenings allows users to evade detection (Gamage et al., 2019). Contrary to initial public perception, the psychoactive properties of these blends stem not from the plant material itself, but from synthetic chemicals sprayed onto the herbs. These active compounds are often named using acronyms representing the researchers or laboratories that first synthesized them – such as JWH (John W. Huffman) or AM (Alexandros Makriyannis) – followed by a numeric code (Liechti, 2015).

In 2017, the European Monitoring Center for Drugs and Drug Addiction (EMCDD) introduced an interactive online model to simplify the complex chemistry of SCs. According to this framework, most synthetic cannabinoids share a modular architecture composed of four distinct structural domains (Fig. 2):

- Core: the central scaffold of the molecule
- Tail: a side chain attached to one side of the core structure
- Link: a functional linking group connecting the core to the outer domain
- Ring: an outer ring substituent bound via the link domain

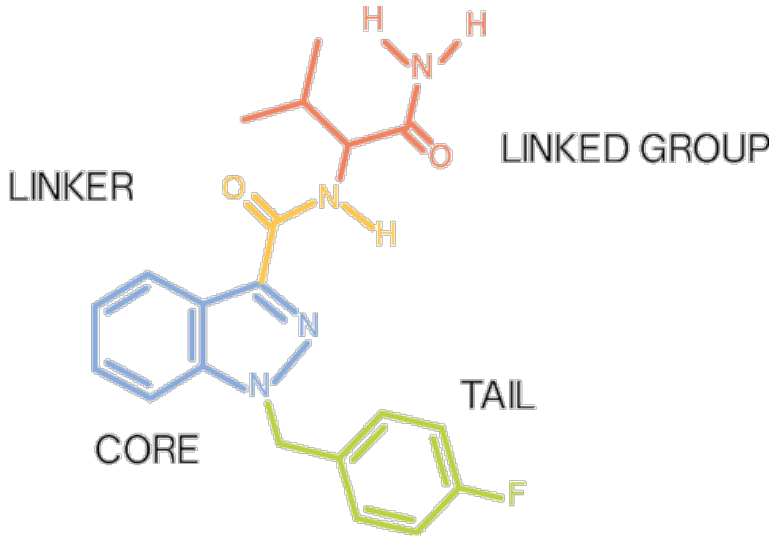


Figure 2. Typical modular architecture of most synthetic cannabinoids (image from https://www.euda.europa.eu/topics/pods/synthetic-cannabinoids_en)

Because each of these four components can be independently substituted with various chemical groups, the number of potential molecular combinations remains very high (EMCDDA, 2017). Structurally, SCs fall into seven major groups: naphthoylindoles (such as JWH-018, JWH-073, and JWH-398), naphthylmethylindoles, naphthoylpyrroles, naphthylmethylindenes, phenylacetylindoles (also termed benzoylindoles, e.g., JWH-250), cyclohexylphenols (e.g., CP 47,497 and its analogs), and classical cannabinoids (e.g., HU-210). APINACA, AKB48, and 5F-AKB48 do not belong to any of the seven traditional structural groups used to classify first-generation synthetic cannabinoids; instead, they belong to the adamantylindole and adamantylindazole classes (Fig. 3) (Uchiyama et al., 2012).

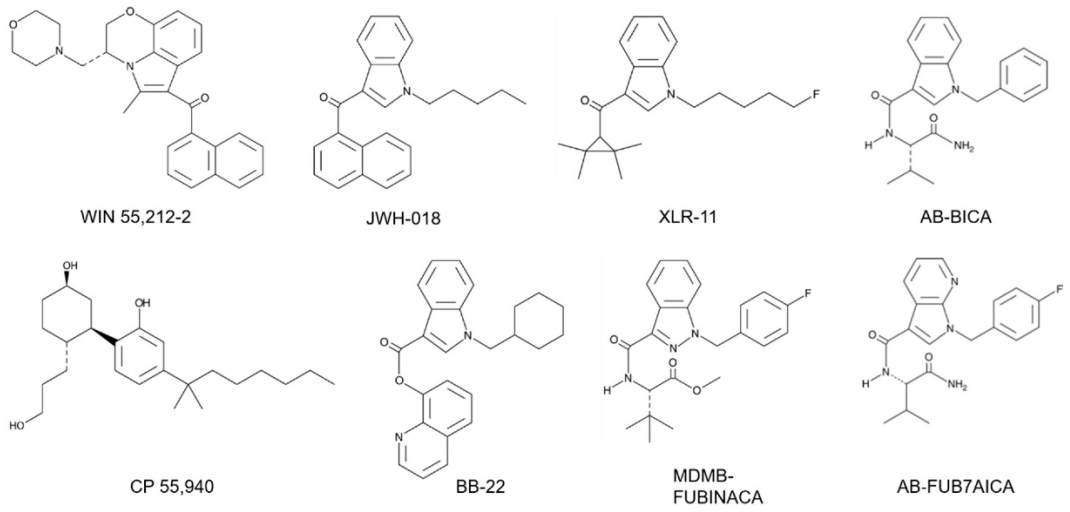


Figure 3. Structural classes of synthetic cannabinoids. (adapted from Walsh and Andersen, 2020)

Like Δ^9-THC, SCs primarily exert their pharmacological effects by targeting cannabinoid system, affecting its receptors, cannabinoid receptor 1 (CB_1R) and cannabinoid receptor 2 (CB_2R). However, unlike THC, which is a partial agonist, most SCs function as full agonists, displaying substantially greater potency and intrinsic efficacy (I. Vardakou et al., 2010; V. Auwarte et al., 2009). While CB_1R is predominantly localized within the central nervous system, it is also expressed at lower, functionally relevant concentrations across various peripheral tissues, including the myocardium, liver, lungs, kidneys, vascular endothelium, and reproductive tract (AC. Howlett et al, 2002; RG. Pertwee et al., 2010). Conversely, CB_2R is mainly concentrated on immune cells, though its presence is also confirmed in the brain and several peripheral organs (JC. Ashton et al., 2006; MD. Van Sickle et al., 2005). Activation of the CB_1 receptor by cannabinoids elicits a distinct profile of psychotropic effects, such as euphoria, heightened sensory perception, analgesia, appetite stimulation, and memory disruption. Stimulation of both CB_1R and CB_2R suppresses adenylyl cyclase activity, which directly regulates the opening and closing of membrane ion channels (R.G Pertwee, 2000). Depending on the specific cell type and ligand involved, CB_1R, and to a lesser extent CB_2R, also triggers several downstream signaling cascades, including the mitogen-activated protein kinase (MAPK) pathway, the PI3K/Akt axis, and ceramide synthesis (A.C Howlett, 2005). The broad presence of cannabinoid receptors throughout different organs, combined with this diverse network of intracellular pathways, provides the primary mechanistic explanation for the wide range of toxicities associated with synthetic cannabinoid use (C.A Gallelli et al., 2018; R. Roque-Bravo et al., 2023). High densities of CB_1 receptors are localized within limbic areas such as the Ventral Tegmental Area (VTA), Nucleus Accumbens (NAc), Ventral Pallidum, and PFC, where synthetic cannabinoids likely regulate reward circuits, addiction vulnerability, and cognitive functions (G.F. Koob and N.D. Volkwow, 2010). Consistent with this mechanism, preclinical rodent models indicate that, similarly to other addictive drugs, these agents modulate mesolimbic dopaminergic signaling (I. Canazza et al., 2016; M.A. De Luca et al., 2015; A. Ossato et al., 2016) and shape conditioned behaviors (G. Di Chiara et al., 2004; C. Miliano et al., 2016). Furthermore, behavioral studies demonstrated that some SCs (such as JWH-018 and AKB48) enhanced spontaneous locomotor activity in mice via mechanisms dependent on CB_1 receptors and dopamine signaling (A. Ossato et al., 2017; G. Corli et al., 2025). Beyond circuit-level behavioral effects, these compounds also exhibit direct neurotoxicity; specifically, synthetic cannabinoids induce apoptosis in primary forebrain neurons through a caspase-3-dependent mechanism mediated selectively by CB_1, rather than CB_2, receptors (K. Tomiyama and M. Funada, 2014). At the intracellular level, while central nervous system responses to cannabinoids are conventionally driven

by CB_1 coupling to inhibitory $G_{i/o}$ proteins, certain synthetic ligands demonstrate profound functional selectivity. For example, the aminoalkylindole agonist WIN 55,212-2 stabilizes a distinct receptor conformation that shifts coupling toward G_q proteins and activates the phospholipase C (PLC) cascade. This pathway stimulates inositol phosphate production and triggers a substantial release of Ca^{2+} from intracellular endoplasmic reticulum stores via both IP_3 and ryanodine receptors, independent of extracellular influx or $G_{i/o}$ signaling (J.E. Lauckner et al., 2005). Consequently, synthetic cannabinoid-induced CB_1 activation can directly disrupt intracellular calcium dynamics, providing a critical mechanistic link between receptor overstimulation and calcium-dependent neurotoxic pathways.

While their parent scaffolds are designed to bind and activate human cannabinoid type-1 (hCB1) receptors, metabolic processing after inhalation or ingestion generates numerous secondary compounds with uncharacterized pharmacological profiles. A significant fraction of these metabolites undergoes hydroxylation on the pentyl chain, a vital functional group that governs both hCB1 binding affinity and receptor selectivity. Consequently, characterizing the biological activity of these metabolic products is crucial for unraveling the overall *in vivo* toxicity and physiological impact of synthetic cannabinoids (Gamage et al., 2019). *In vitro* models using human and rat hepatocytes or liver microsomes consistently show that terminal pentyl chain hydroxylation yields the most abundant metabolites across diverse compounds, including CUMYL-PICA (Kevin et al., 2017), 5F-MN-18 (Carlier et al., 2018), AB-PINACA (Takayama et al., 2014), AMB, 5F-AMB (Andersson et al., 2016), and EG-018 (Mogler et al., 2018). Crucially, the presence of these hydroxypentyl derivatives in human urine samples confirms their real-world *in vivo* formation in consumers (Wohlfarth et al., 2015).

1.3 JWH-018

The naphthoylindole JWH-018 (1-pentyl-3-(1-naphthoyl)indole) (Fig. 4) gained widespread attention in December 2008 when the German company THC Pharma (Frankfurt) identified it as an active ingredient in the herbal blend "Spice". Shortly thereafter, detailed structural analyses by research groups at the University of Freiburg further confirmed the presence of synthetic cannabinoids in these products, marking JWH-018 as the first synthetic cannabinoid officially identified in Europe (EUDA, 2017). Compared to Δ^9-THC, JWH-018 displays a significantly higher binding affinity for CB_1 receptors. Consequently, it induces far more severe physiological and behavioral disruptions, including marked alterations in motor activity, sensorimotor gating, body temperature, nociception, and respiratory rate (Ossato et al., 2015; Vigolo et al., 2015). Beyond standard cannabimimetic effects, JWH-018 exhibits distinct psychostimulant properties:

- Acute low-dose effects (0.3 mg/kg): triggers spontaneous hyperlocomotion in rodent models alongside elevated dopamine release in the striatum and nucleus accumbens (Ossato et al., 2017).
- Dopaminergic and CB_1 dependence: This acute hyperactivation relies on integrated CB_1 and dopaminergic pathways, as it is selectively blocked by:
    - The CB_1 inverse agonist/antagonist AM251
    - The $D_{1/5}$ receptor antagonist SCH23390
    - The $D_{2/3}$ receptor antagonist haloperidol
- Chronic high-dose effects (6 mg/kg): Repeated administration of the synthetic cannabinoid JWH-018 (6 mg/kg, i.p.) progressively enhances spontaneous locomotion and triggers aggressive behavior in mice. These behavioral alterations are driven by CB_1 receptor activation paired with downstream dopaminergic mechanisms (G. Corli et al., 2025).

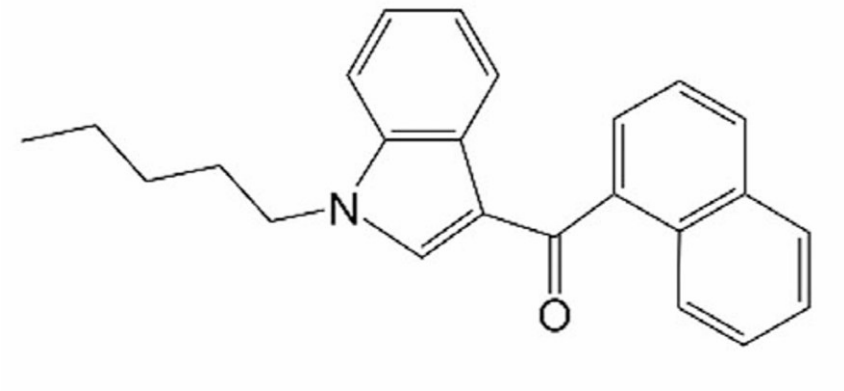


Figure 4. Chemical structure of JWH-018 (image adapted from B.K Atwood et al., 2010)

It is well-known that hydroxylation is a common way of the metabolic transformation of xenobiotics as it facilitates their elimination from an organism by glucuronidation (or sulfation) of the hydroxylated metabolites. Based on the data reported for a JWH analog, it was natural to anticipate that the in vivo metabolism of JWH-018 should occur similarly (Q. Zhang et al., 2006).

The unchanged parent drug JWH-018 remains undetected in post-administration urine below 50 pg/mL. Following derivatization (trimethylsilylation adding 88 amu) and enzymatic hydrolysis, required because these targets are heavily glucuronidated, GC–MS/MS revealed two low-abundance monohydroxylated metabolites ($[M]^+ = 429$ amu): M1 and M2 (T. Sobolevsky et al., 2010). Both metabolites retain an unmodified naphthalenyl core, evidenced by characteristic fragment ions at m/z 127 and 155. However, distinct MS/MS fragmentation patterns differentiate their hydroxylation

sites: M1 (Indole ring-hydroxylated) produces a m/z 324 fragment via the sequential loss of trimethylsilanol (90 amu) and an alkyl methyl group, a cleavage pattern characteristic of indole phenyl ring modification; conversely M2 (N-alkyl-hydroxylated) òacks the m/z 324 transition in SRM mode, indicating hydroxylation occurs on the N-alkyl side chain rather than the indole core (T. Sobolevsky et al., 2010). LC–MS/MS identifies M1 (monohydroxylated) as the primary metabolite, alongside minor derivatives: carboxylated M4, dihydroxylated M6/M7, reduced di/tri-hydroxylated M8–M11, and N-despentyl variants M12/M13 (T. Sobolevsky et al., 2010).

1.4 The Endocannabinoid System

Over the past quarter-century, the endocannabinoid system (ECS) has been recognized as a vital neuromodulatory framework. Anatomically and functionally, the ECS consists of three core components (Fig. 5):

i. Endogenous cannabinoids**:** lipid-based signaling molecules (endocannabinoids).
ii. cannabinoid receptors**:** primary molecular targets that mediate ECS signaling.
iii. metabolic enzymes**:** proteins dedicated to the biosynthesis and enzymatic degradation of endocannabinoids.

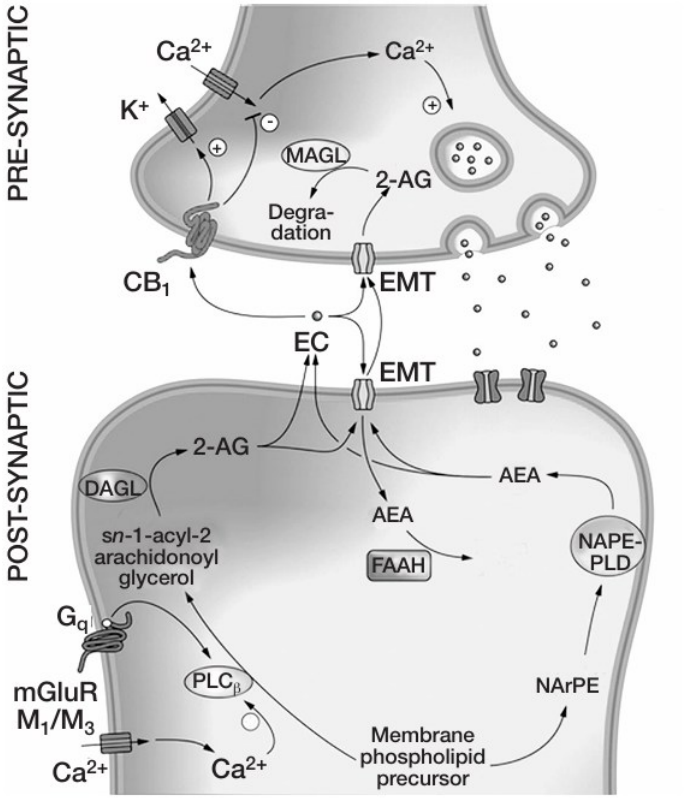


Figure 5. Representation on the synthesis, signalling and degradation of endocannabinoids at the synaptic site (image adapted from Marsicano and Lutz, 2006)

Endocannabinoids are naturally occurring lipid-based signaling molecules that activate cannabinoid receptors, producing behavioral shifts that partially mirror the effects of Δ^9-tetrahydrocannabinol (Δ^9-THC), the main psychoactive component of cannabis.

The two best-characterized endocannabinoids are anandamide (arachidonoylethanolamide) and 2-arachidonoylglycerol (2-AG). Unlike classical neurotransmitters, which are pre-packaged into synaptic vesicles, endocannabinoids are synthesized "on demand" from cell membrane precursors. Depolarization or G-protein-coupled receptor activation triggers their rapid enzymatic release directly into the extracellular space. Properties differ significantly between the two key ligands: 2-AG acts as a full, high-efficacy agonist at both CB_1 and CB_2 receptors, while anandamide functions as a partial, low-efficacy gonist at CB_1 and displays minimal efficacy at CB_2; in addition, in system with low receptor density or poor signaling coupling, anandamide can also act as an antagonist by competing with higher-efficacy ligands. The metabolic pathways governing the synthesis and regulation of anandamide and 2-AG are fundamentally distinct, relying on specialized enzymatic machinery that dictates their unique physiological roles. While both compounds share arachidonic acid as a structural

constituent, their synthesis, tissue distribution, and functional implications within the central nervous system differ significantly (P. Pacher et al., 2006). Compared to anandamide, the enzymatic generation of 2-AG proceeds through a relatively streamlined pathway where membrane-bound phosphatidylinositol bisphosphate is cleaved by phospholipase C to yield diacylglycerol, which is subsequently hydrolyzed by diacylglycerol lipase ("DAGL") to liberate 2-AG.

DAGL exists in two isoforms, $DAGL_{\alpha}$ and $DAGL_{\beta}$. DAGLα drives the majority of 2-AG production responsible for retrograde synaptic plasticity in the adult brain, anchored within dendritic spines in close physical proximity to group I metabotropic glutamate receptors and directly apposed to presynaptic CB_1 terminals; conversely, DAGLβ primarily operates during immune responses. Crucially, 2-AG is not merely an endocannabinoid ligand; it serves as a central metabolic intermediate in general lipid synthesis, acting as the major donor of arachidonic acid for prostaglandin production in the brain, liver, and lungs (D.K. Namura et al., 2011). In contrast, anandamide synthesis is far more heterogeneous and region-dependent, occurring via at least four distinct enzymatic routes starting from N-arachidonoyl phosphatidylethanolamine (NAPE) (H.C. Lu and K. Mackie, 2016). Anandamide and 2-AG are cleared and inactivated through distinct enzymatic networks (B.F Cravatt et al., 1996). Anandamide degradation is primarily driven by fatty acid amide hydrolase (FAAH), an enzyme that also hydrolyzes other non-cannabinoid lipid mediators like palmitoylethanolamide and oleoylethanolamide. As a result, pharmacological inhibition of FAAH elevates a broad spectrum of bio-active ethanolamides, triggering widespread responses beyond the endocannabinoid system. Alternatively, anandamide can be oxidized by cyclooxygenase-2 (COX-2) to yield prostamides, which possess distinct pharmacological actions and play a key role in treating intraocular hypertension (D.F Woodward et al., 2008).

In contrast, 2-AG clearance is distributed across three main hydrolytic enzymes, monoacylglycerol lipase (MAGL), α/β-hydrolase domain 6 (ABHD6), and α/β-hydrolase domain 12 (ABHD12) (J.L Blankman et al., 2007). Finally, 2-AG is also oxidized by COX-2 into prostaglandin E_2-glycerol esters (D.J. Hermanson et al., 2014).

1.4.1 Cannabinoid receptors

Endocannabinoids act largely through CB_1 and CB_2 receptors, both G_i/G_0-coupled GPCRs that suppress adenylyl cyclase, block voltage-gated calcium entry, and trigger inwardly rectifying potassium channels alongside MAP kinase cascades to regulate synaptic release, gene expression, and cell movement (A.C. Howlett et al., 2002). Beyond classical cannabinoid receptors, non-canonical targets such as TRPV1 channels and nuclear PPAR-α/γ receptors also mediate endocannabinoid actions,

particularly for anandamide and structurally related acyl ethanolamides. CB_1 receptors are densely distributed throughout the CNS, concentrating pre-synaptically along axon terminals outside the active zone across the cortex, basal ganglia, hippocampus, and cerebellum, with peak expression occurring on cholecystokinin-positive GABAergic interneurons and striatal medium spiny neurons alongside functionally vital lower levels in glutamatergic populations and glial cells (G. Nyiri et al., 2005; K. Mackie, 2005). In contrast, CB_2 receptors remain sparse under basal conditions, primarily localized to microglia and vascular elements, yet they display remarkable inducibility, surging up to 100-fold during neuroinflammation or tissue damage either through local cellular upregulation or the infiltration of peripheral immune cells (M.D. Van Sickle et al., 2005). The presynaptic distribution of CB_1 receptors, combined with their capacity to suppress neurotransmitter release, complements the postsynaptic localization of endocannabinoid-synthesizing enzymes. Because postsynaptic events like intracellular calcium surges or $G_{q/11}$-coupled GPCR activation trigger the synthesis of endocannabinoids (most notably 2-AG), these signaling lipids act as retrograde messengers that travel backward across the synapse to regulate presynaptic activity (M. Kano et al., 2009). This retrograde mechanism drives three primary forms of short- and long-term synaptic plasticity:

i. Depolarization-induced suppression, a transient inhibition of GABAergic (depolarization-induced suppression of inhibition, DSI) or glutamatergic (depolarization-induced suppression of excitation, DSE) transmission initiated by postsynaptic depolarization;
ii. Metabotropic-induced suppression**,** short-term depression of inhibitory (MSI) or excitatory (MSE) inputs triggered via postsynaptic G-protein-coupled receptor activation.
iii. Endocannabinoid-mediated long-term depression **(**eCB-LTD**):** Persistent, long-lasting reduction in neurotransmitter release driven by sustained presynaptic CB_1activation(Fig.6)(M.Kano et al., 2009).

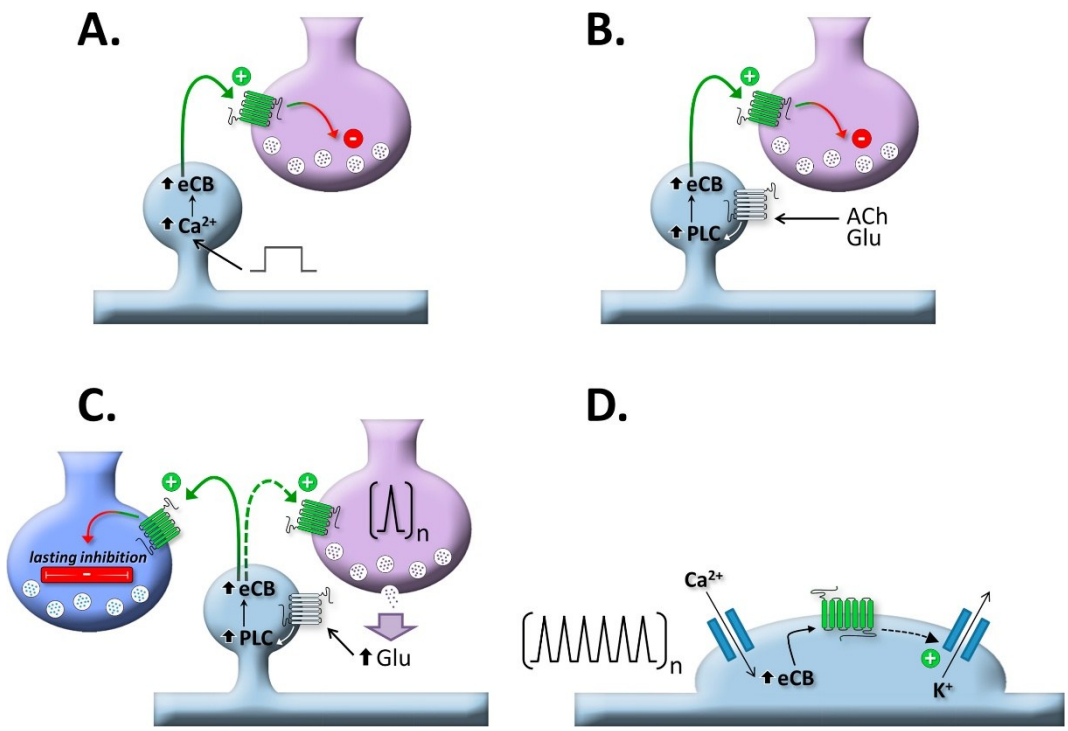


Figure 6. Modes of endocannabinoid-mediated synaptic and intrinsic regulation: (A) DSE/DSI. (B) MSE/MS. (C) eCB-LTD. (D) SSI. (Image adapted from Hui-Chen Lu and Ken Mackie, 2016)

Both THC and anandamide function as low-efficacy partial agonists at CB_1 receptors, whereas 2-AG is a high-efficacy full agonist (T. Luk et al., 2004). In brain regions with low CB_1 receptor density or limited downstream effector coupling, low-efficacy ligands (THC or anandamide) compete with 2-AG, effectively acting as functional antagonists by blunting robust 2-AG-driven signaling. Conversely, in regions with high receptor reserves or tight effector coupling, THC acts as a classic agonist to depress synaptic transmission (H.C. Lu & K. Mackie, 2016).

Synthetic cannabinoids found in preparations like "Spice" possess high intrinsic efficacy and potent agonist activity at CB_1. Unlike the self-limiting partial agonism of natural THC, these potent synthetic agents produce a significantly higher incidence of severe adverse psychiatric events and toxicities (J. van Amsterdam et al., 2015).

1.5 Calcium Ions And The Central Nervous System

1.5.1 Role of calcium in the central nervous system

Calcium ions (Ca^{2+}) are essential regulators of physiological processes within the central nervous system. In neurons, intracellular calcium signaling is integral to neurotransmission, stabilizing membrane potential, controlling neuronal excitability, and mediating depolarizing signal transduction. As universal second messengers, these ions contribute directly to synaptic activity, memory formation, and learning mechanisms (D. Pikor et al., 2024). Elevations in cytosolic calcium levels occur through extracellular influx across the plasma membrane or mobilization from intracellular stores, triggered by membrane depolarization or receptor activation. The entry of calcium into neurons is mediated by plasma membrane receptors and voltage-gated ion channels. These channels are critical for nervous system function, controlling key processes such as neuronal depolarization and neurotransmitter release. Dysfunctions in calcium channel subunits due to genetic mutations, termed channelopathies, are implicated in various neurological conditions, including migraine. Furthermore, an impaired ability to maintain calcium homeostasis is a feature of neurodegenerative diseases such as Alzheimer's, Parkinson's, and Huntington's diseases, as well as epilepsy (D. Pikor et al., 2024). Maintaining a stable calcium balance, known as calcium homeostasis, is essential for normal nervous system function. In nerve cells, these ions are involved in key processes, including action potentials, where membrane depolarization opens voltage-gated calcium channels to allow Ca^{2+} entry and signal transmission between neurons, where this rapid influx at the axon terminal triggers synaptic vesicles to release neurotransmitters into the synaptic cleft. They also participate in synaptic plasticity, cell signaling, and programmed cell death (apoptosis). However, if this balance is disrupted and too much Ca^{2+} enters the cell, it can cause excitotoxicity and cell death, leading to nerve damage (D. Pikor et al., 2024). To prevent this, specific buffering proteins such as parvalbumin and calreticulin bind excess intracellular calcium to keep levels safe (M. Yanez et al., 2012). Additionally, calcium can bind to specialized proteins such as calmodulin (calcium-dependent protein kinase), regulating learning and memory pathways or to synaptotagmin 9 (SYT9), acting as a calcium sensor that helps release neurotransmitters into the synaptic cleft (M.J. Seibert et al., 2023). Neuronal communication relies directly on ion flow across the cell membrane, with Ca^{2+} serving as a central trigger. When an action potential reaches the presynaptic terminal, it opens voltage-gated calcium channels (VGCCs), causing a rapid entry of extracellular Ca^{2+} into the terminal cytoplasm (A.C. Dolphin, 2021; J. Heck et al., 2021).

This sudden rise in local Ca^{2+} stimulates synaptic vesicles to fuse with the presynaptic membrane, a mechanism coordinated by SNARE complex proteins, specifically v-SNAREs located on the vesicle surface and t-SNAREs anchored to the target plasma membrane (J. Malsam et al., 2008). Membrane fusion releases neurotransmitters into the synaptic cleft, where they bind to specific postsynaptic receptors. This receptor binding alters the postsynaptic membrane potential, opening voltage-gated Na^{+} channels to generate a new action potential and propagate the nerve impulse. Because neurotransmitter exocytosis is highly dependent on calcium dynamics, presynaptic Ca^{2+} concentrations directly govern the strength, timing, and plasticity of synaptic transmission across neural networks (A.C. Dolphin et A. Lee, 2021; E. Neher et T. Sakaba, 2008). Beyond its function in neurotransmitter exocytosis, calcium acts as a crucial second messenger that regulates numerous intracellular signaling pathways and essential cell functions (E. Carafoli et M. Crompton, 1978). Upon entering the cell, Ca^{2+} binds to specific calcium-binding proteins (CaBPs), especially calmodulin, which triggers diverse downstream pathways. Because hundreds of target proteins contain calmodulin-binding sites, they remain under direct calcium control (D.E. Clapham, 2007). Activated calmodulin functions like a molecular switch, modulating various enzymes, kinases, phosphatases, and ion channels (D.E Clapham, 2007; F.C. Stevens, 1983). A prominent example involves calcium/calmodulin-dependent protein kinases (CaMKs), which are abundant in the brain, particularly within the hippocampus. CaMKs play a critical role in synaptic plasticity, the activity-driven strengthening or weakening of synapses that underlies learning and memory formation. This plasticity relies on two opposing mechanisms: long-term potentiation (LTP), which strengthens synaptic connections, and long-term depression (LTD), which reduces synaptic strength (T. Nagase et al., 2003; J.A. Connor et al., 1999).

1.5.2 Calcium homeostasis in neurons

Maintaining precise intracellular Ca^{2+} homeostasis is essential for neuronal function and survival, as prolonged or excessive accumulation causes cytotoxic damage. To sustain physiological signaling while avoiding cell injury, neurons strictly regulate cytosolic calcium concentrations through several specialized entry pathways. Membrane depolarization during action potentials opens VGCCs, allowing rapid calcium entry that drives neurotransmitter exocytosis and initiates synaptic plasticity pathways. In parallel, postsynaptic NMDA receptors allow direct calcium influx upon simultaneous glutamate binding and membrane depolarization (J.A. Connor et al., 1999; C. Luscher et R.C. Malenka, 2012). In addition to these classical routes, transient receptor potential (TRP) channels serve as multimodal entry pathways activated by diverse external and internal stimuli (N.J. Himmel et D.N. Cox,

2020). For example, thermal changes recruit specific channels, heat activates TRPV1 while cold triggers TRPM8, and mechanical forces are sensed by channels such as TRPA1 and TRPC1. Furthermore, chemical compounds like capsaicin stimulate TRPV1 and environmental irritants activate TRPA1, while TRPM2 channels open in response to oxidative stress to modulate calcium levels during cellular stress conditions (N.J. Himmel et D.N. Cox, 2020). The endoplasmic reticulum (ER) serves as the primary intracellular reservoir for Ca^{2+} in neurons. Calcium mobilization from the ER into the cytoplasm occurs through two main receptor systems located on its membrane: first, inositol 1,4,5-trisphosphate receptors (IP_3Rs), open in response to intracellular signaling cascades initiated by neurotransmitters such as glutamate and acetylcholine; binding of IP_3 to these receptors directly releases stored Ca^{2+}; second, ryanodine receptors (RyRs) mediate calcium-induced calcium release (CICR), a process in which a localized initial entry of extracellular Ca^{2+}, for example, via voltage-gated channels, binds to RyRs and amplifies the cytosolic signal by triggering a larger efflux of calcium from the ER lumen (J. Heck et al., 2021; E. Carafoli et M. Crompton, 1978; M. Gleichmann et M.P. Mattson, 2011). Mitochondria function as essential dynamic calcium buffers during sustained or intense neuronal activity. When cytoplasmic Ca^{2+} levels rise significantly, mitochondria sequester the excess ions via the mitochondrial calcium uniporter (MCU), preventing dangerous intracellular overload. This mitochondrial calcium uptake also enhances metabolic activity by stimulating key enzymes involved in ATP synthesis, matching energy production to the elevated metabolic demands of active neurons. As neuronal stimulation subsides, mitochondria gradually export the accumulated Ca^{2+} back into the cytosol or toward other storage organelles to restore resting equilibrium (M.R. Duchen, 2000). Neurons prevent cytotoxic calcium overload through a combination of intracellular buffering proteins and active clearance pumps. Within the cytoplasm, calcium-binding proteins such as calbindin, parvalbumin, and calretinin rapidly bind free Ca^{2+} to suppress sudden fluctuations in concentration. Concurrently, membrane transporters remove excess calcium from the cytosol to restore baseline levels. Across the plasma membrane, the plasma membrane Ca^{2+}-ATPase (PMCA) consumes ATP to maintain low resting calcium concentrations, while the sodium–calcium exchanger (NCX) uses the electrochemical sodium gradient to rapidly export calcium after action potentials and synaptic events. Within the intracellular compartment, the sarco/endoplasmic reticulum Ca^{2+}-ATPase (SERCA) pump returns cytosolic calcium back into the endoplasmic reticulum lumen, replenishing internal stores and maintaining global calcium homeostasis (A. Britzolaki et al., 2018).

1.5.3 Effects of synthetic cannabinoids on intracellular calcium levels

Cannabinoid-mediated synaptic modulation has traditionally been viewed through the lens of retrograde signaling, in which target cells release endocannabinoids to suppress presynaptic neurotransmitter release by dampening calcium influx (Alger 2002; Hoffman and Lupica 2000; Kreitzer and Regehr 2001; Sullivan, 1999). In several neural circuits, such as hippocampal inhibitory networks, striatal excitatory terminals, and trigeminal neurons, this presynaptic inhibition was initially attributed almost exclusively to the blockade of N-type VGCC via CB_1 receptor active (Huang et al. 2001; Liang et al. 2004). Other optical and electrophysiological analyses, however, broadened this perspective by demonstrating that presynaptic CB_1R stimulation in cerebellar granule cell boutons suppresses calcium entry across a wider spectrum of high-voltage-activated channels, simultaneously attenuating N-, P/Q-, and R-type currents to reduce excitatory postsynaptic potentials (Brown et al. 2004). Whole-cell patch-clamp analyses reveal that, alongside presynaptic modulation, synthetic and endogenous cannabinoids inhibit P-type calcium currents in isolated rat Purkinje cells (PCs) without requiring CB_1R engagement (A. Fisyunov et al., 2006). Using primary hippocampal cultures monitored via high-sensitivity Ca^{2+} fluorescence spiking and microelectrode arrays (MEAs), both benchmark synthetic cannabinoids (such as WIN 55,212-. 2, HU-210, CP 55,940, and JWH-018) and diverse emerging structural analogues (including XLR-11, JWH-250, 5F-PB-22, AB-PINACA, and MAM-2201) produce robust, rapid, and concentration-dependent suppression of spontaneous neural electrical activity. In particular, naphthoylindole derivatives like JWH-018 inhibit hippocampal Ca^{2+} spiking frequencies at micromolar concentrations in a manner fully reversible by the selective CB_1 antagonist rimonabant (J.S. Tauskela et al., 2016). In sharp contrast to this canonical dynamics, specific synthetic cannabinoids can subvert classical receptor coupling to trigger pathological intracellular calcium surges. While CB_1 receptors preferentially signal through $G_{i/o}$ cascades, the aminoalkylindole agonist WIN 55,212-2 displays ligand-biased functional selectivity by stabilizing an alternative active receptor conformation that couples directly to G_q proteins. As demonstrated in both CB_1-expressing HEK293 cells and cultured hippocampal neurons, exposure to WIN 55,212-2 evokes a rapid, robust elevation of cytosolic Ca^{2+} reaching several hundred nanomolar, an effect fully sensitive to the CB_1 antagonist SR141716A, and absent upon treatment with classical cannabinoids like Δ^9-THC, CP 55,940, or 2-arachidonoylglycerol (J.E. Lauckner et al., 2005). This receptor-mediated rise in Ca^{2+} is independent of $G_{i/o}$ signaling and extracellular entry. Instead, the calcium surge is driven by a G_q/phospholipase C cascade that stimulates inositol phosphate turnover and mobilizes Ca^{2+} from

sarco/endoplasmic reticulum stores via IP_3 and ryanodine receptor (J.E. Lauckner et al., 2005). This aberrant intracellular calcium surge provides a critical mechanistic foundation for the cellular toxicity, mitochondrial stress, and caspase-3-dependent neuronal apoptosis characteristic of high-potency synthetic cannabinoid exposure.

2 CENTRAL NERVOUS SYSTEM: CEREBRAL CORTEX, DORSAL STRIATUM AND CEREBELLUM

The central nervous system of the mouse follows the standard mammalian body plan, developing from the embryonic neural tube and organizing along its main longitudinal axis into well-defined anatomical divisions (Schröder et al., 2020). Moving from the caudal to the cranial end, the murine CNS comprises the spinal cord (ending caudally in the cone-shaped *conus medullaris*), the brainstem (medulla oblongata, pons, and mesencephalon) associated with the cerebellum, the diencephalon (thalamus and hypothalamus), and the telencephalon, which encompasses the cerebral cortex, hippocampus, amygdala, caudate-putamen, and olfactory system (Fig. 7) (Schröder et al., 2020). The entire neuraxis is housed within and protected by the axial skeleton, specifically the neurocranium and the vertebral canal formed by 7 cervical, 13 thoracic, 6 lumbar, 4 sacral, and approximately 28–30 caudal vertebrae (Treuting et al., 2012). Compared to the human skull, the murine cranium is markedly elongated anteroposteriorly to accommodate the expansive nasal cavity and vomeronasal organ, presenting lateral orbits and an occipital foramen magnum directed horizontally along the longitudinal body axis, a feature consistent with quadrupedal locomotion (Treuting et al., 2012). Beneath the protective bony casing, the nervous tissue is shielded by three connective tissue membranes: the outer tough dura mater, the intermediate arachnoid mater, and the delicate pia mater, which adheres directly to the neural parenchyma (Schröder et al., 2020). In addition, the brain is suspended in cerebrospinal fluid (CSF) actively produced by the choroid plexus located within the lateral, third, and fourth ventricles (Schröder et al., 2020). This fluid circulates through the internal brain ventricles and moves through small openings into the surrounding subarachnoid space to provide mechanical cushioning, maintain physiological intracranial pressure, regulate interstitial ion balance, and facilitate the clearance of metabolic waste via the glymphatic pathway (Jessen et al., 2015; Schröder et al., 2020). From a spatial perspective, mouse neuroanatomy relies on an orthogonal Cartesian system of three perpendicular planes and axes, horizontal, coronal, and sagittal, where in any target point within the brain can be precisely defined by three coordinates anchored to cranial landmarks like Bregma and Lambda and derived from stereotaxic atlases, which compile histological sections along these planes to guide experimental, imaging, and surgical procedures (Paxinos & Franklin, 2019). Beyond its gross layout, the murine brain exhibits marked morphological differences compared to the human brain; most notably, the mouse cerebral cortex is lissencephalic (smooth and devoid of sulci and gyri) while preserving a canonical six-layered laminar cytoarchitecture, and the olfactory bulbs are disproportionately large, reflecting the vital reliance of this macrosmatic species on olfactory cues for foraging and social

dynamics (Herculano-Houzel et al., 2006). Furthermore, the murine hippocampus (consisting of the dentate gyrus, CA1–CA3 fields, and subiculum) curves dorsomedially beneath the cortex in an accessible crescent-like orientation rather than occupying a ventromedial temporal position as in humans, and the primary somatosensory cortex possesses a specialized "barrel cortex" in layer IV whose cylindrical cell clusters correlate topographically with individual contralateral facial vibrissae (Petersen, 2007; Strange et al., 2014). At the microscopic level, the murine CNS parenchyma is organized into diverse neuronal populations, predominantly excitatory glutamatergic projection neurons and local inhibitory GABAergic interneurons, closely integrated with non-neuronal glial compartments (Paxinos & Franklin, 2019). These include astrocytes, which extend perivascular end-feet to form the blood-brain barrier and regulate ionic and neurotransmitter homeostasis; oligodendrocytes, which synthesize myelin sheaths to ensure saltatory axonal conduction and metabolic support; and yolk-sac-derived microglia, which perform continuous immune surveillance, drive neuroinflammatory responses, and remodel synapses via synaptic pruning (Allen & Eroglu, 2017; Colonna and Butovsky, 2017; Simons and Nave, 2016). Together, these cellular networks support broad behavioral and physiological functions: the neocortex and basal ganglia drive voluntary movement, motor habits, and sensorimotor processing; the hippocampus coordinates spatial navigation and memory consolidation; the amygdala orchestrates emotional and threat-related behaviors; the hypothalamus acts as the neuroendocrine and autonomic master regulator; and the cerebellum and brainstem integrate balance, motor coordination, and vital autonomic reflexes including respiration and cardiovascular control (Schröder et al., 2020).

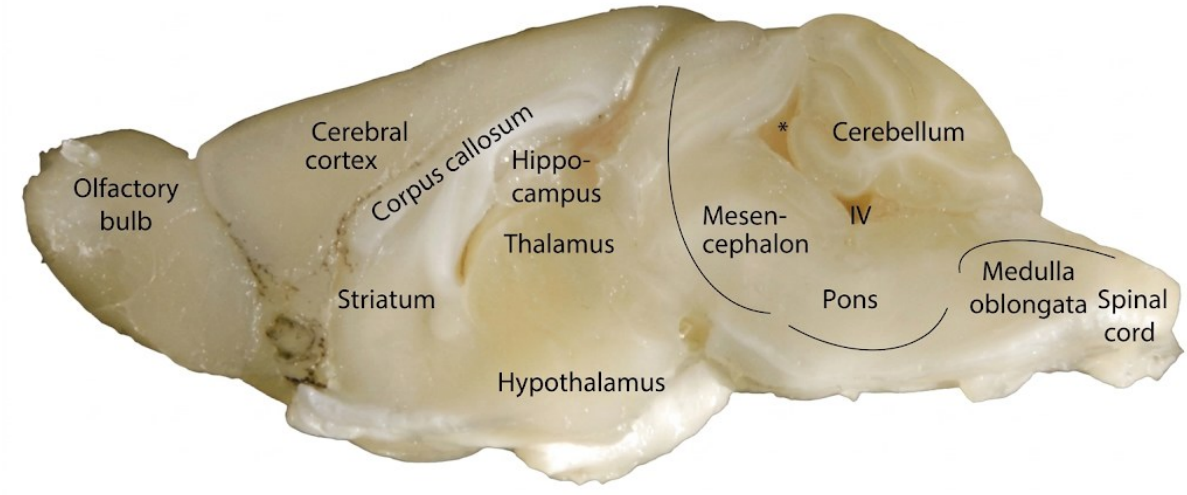


Figure 7. Midsagittal view of the mouse central nervous system (image adapted from Schröder et al., 2020)

2.1 Gross Morphology And Cellular Organization Of The Cerebral Cortex

The cerebral cortex in the mouse acts as an outer shell, covering deep brain regions like the caudate putamen, amygdala, parts of the hypothalamus, thalamus, epithalamus, and sections of the midbrain. Most of it is organized into the classic six-layered neocortex, split functionally into primary, secondary, and tertiary zones. Here, sensory areas handle sight, sound, touch, and taste, while the primary motor cortex directs voluntary movement down through the corticospinal tract.

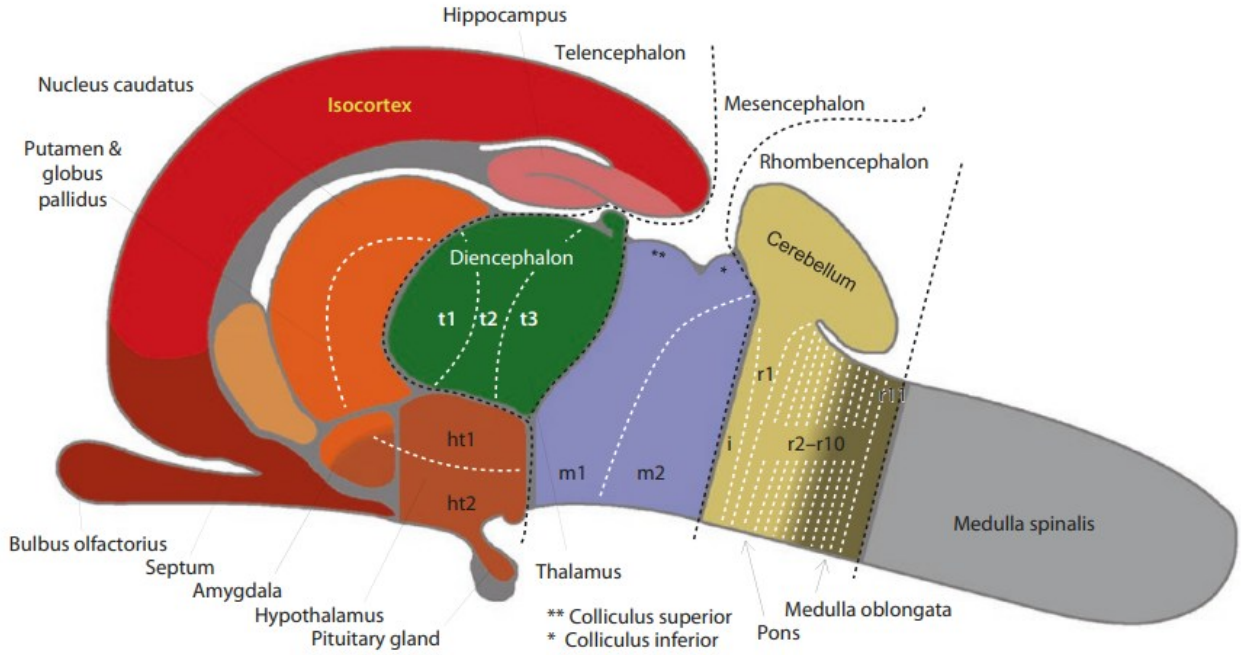


Figure 8. Structural organization of the mammalian brain. The isocortex (cerebral cortex) forms the bulk of the telencephalon, flanked by the hippocampus and olfactory bulb (adapted from Schröder et al., 2020).

Layer formation follows a strict chronological order: deeper-layer neurons projecting down to targets like the thalamus or spinal cord are born first, followed by upper-layer neurons that wire up connections between different cortical areas. Much like the rest of the central nervous system, the neocortex consists of two primary neuronal populations: projection neurons and interneurons. Projection neurons send their axons outside their local area to connect with other cortical regions or subcortical targets. This group comprises two main excitatory cell types, pyramidal neurons and spiny stellate cells, both of which rely on glutamate for neurotransmission. Cortical interneurons encompass a diverse set of cell types that universally utilize GABA as an inhibitory neurotransmitter. Beyond their GABAergic nature, these cells are commonly classified via immunohistochemistry according to their expression of specific calcium-binding proteins, such as parvalbumin, calbindin, and calretinin. In a

landmark study combining electrophysiological recordings with morphological reconstructions, researchers systematically mapped interneuron diversity across layers I, II/III, and V of the adult mouse primary visual cortex (V1). Their analysis identified 15 distinct interneuron subtypes, several of which align directly with the classical Golgi-staining classifications originally described by Ramón y Cajal (1911) (Jiang et al., 2015) (Table 1).

INTERNEURON SUBTYPE	**CORTICAL LAYER LOCALIZATION**
Cajal-Retzius cell	I
Basket cell	II/III/V
Bitufted cell	II/III
Bipolar cell	II/III
Chandelier cell	II/III
Deep-projecting cells	V
Double bouquet cell	II/III
Elongated neurogliaform cell	I
Horizontally elongated cell	V
Martinotti cell	II/III/V
Neurogliaform cell	II/III/V
Shrub cell	V
Single bouquet cell	I

Table 1. Classification of 15 distinct interneuron subtypes in mouse primary visual cortex (Jiang et al., 2015)

The human telencephalon is organized into four main lobes, (i) frontal, (ii) parietal, (iii) temporal, and (iv) occipital, which are bounded by consistent anatomical sulci. Each lobe takes its name from the overlying cranial bones, which are shared by both humans and mice. However, the critical distinction lies in their surface anatomy: while the human cortex features extensive folding, the lissencephalic rodent brain is completely smooth, lacking both gyri and sulci (Fig. 9).



A



B

Figure 9. Comparison between the human brain (A) and the lissencephalic mouse brain (B) (image adapted from Schröder et al., 2020)

Consequently, rodent cortical mapping relies on stereotaxic atlases, cytoarchitectonics, and quantitative methods such as the Gray Level Index (GLI) (Wree et al. 1983; Paxinos, 2014) and cytochrome oxidase histochemistry, which readily highlights metabolic landmarks like the barrel cortex (S1BF). Despite structural differences, rodent cortex parcellation retains human-derived lobar nomenclature, categorizing dorsal pallial derivatives into six main regions: frontal, parietal, temporal, occipital, cingulate, and insular cortices (Schröder et al., 2020).

2.1.1 Motor cortex

From a hierarchical perspective, the motor cortex sits at the top of the motor control system. In humans, the primary motor cortex (MOp) (Brodmann area 4) serves as the main command center for voluntary action, transmitting signals downward via the corticospinal tract. Rodents also possess a functional primary motor cortex and a corticospinal tract, although with a simpler anatomical organization than that seen in primates (Fig. 10) (Schröder et al., 2020).

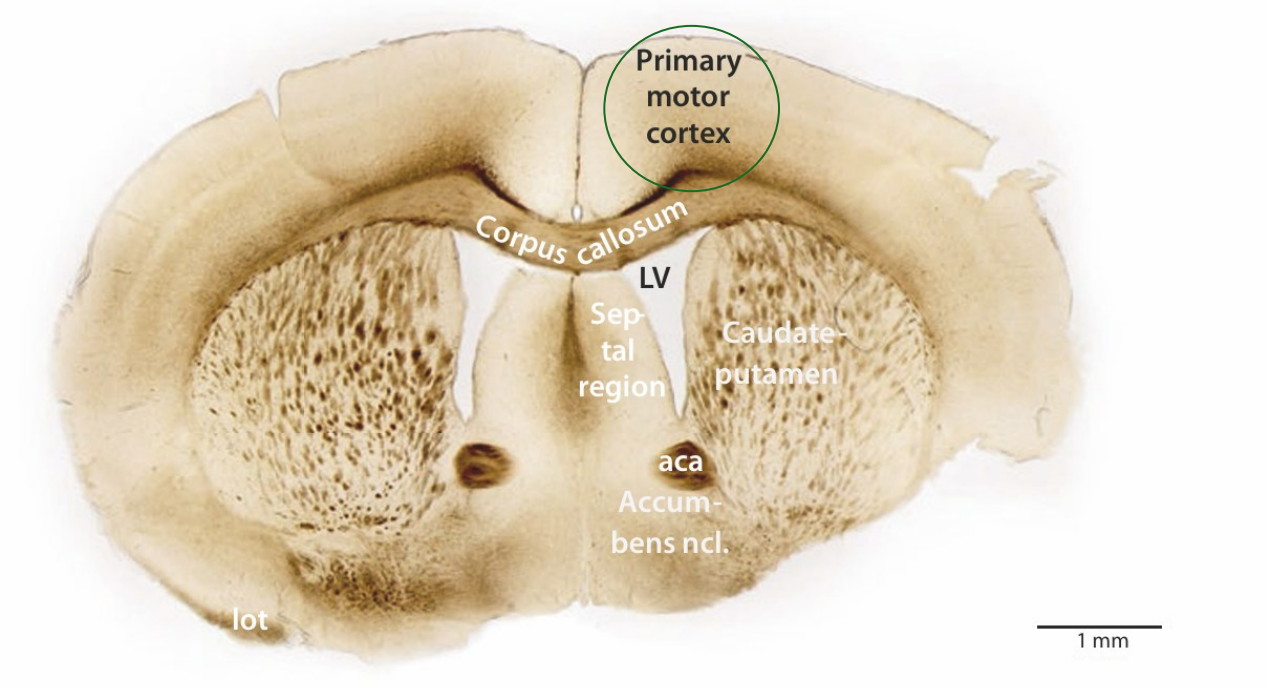


Figure 10. Coronal section of the mouse brain (image adapted from Schröder et al., 2020)

The primary motor cortex, situated within the posterior precentral area (Wree et al., 1983), serves as the origin of the corticospinal tract. While defining "voluntary" movement in nonhuman mammals remains nuanced, an intact MOp and a functional corticospinal tract are essential for executing coordinated somatomotor actions across mammalian species. Like the somatosensory cortex, MOp is organized somatotopically: the large whisker (vibrissal) representation occupies the most cranial position, flanked caudally by smaller fields controlling the fore- and hindlimbs, while the motor representations of the jaw and tongue are located ventrally. The secondary motor cortex (MOs), embedded in the anterior precentral zone, serves as the central integrative node within the motor hierarchy. Positioned rostral to MOp, it directly targets the primary motor cortex via robust efferent projections (Hooks et al. 2011). Murine tracing reveals that primary sensory inputs, such as visual, auditory, and caudal primary somatosensory streams, converge upon high-order associative territories, linking MOs with retrosplenial, parietal, anterior cingulate, and orbitofrontal regions (Barthas and Kwan, 2017).

Functionally, MOs is heavily recruited during context-contingent behavior, governing motor programs triggered by sensory cues, temporal constraints, or preceding movement history. This operational profile aligns seamlessly with its dual connectivity: motor efferents channel executive commands to shape the response, while reciprocal sensory networks continuously feed the area with relevant environmental context (Barthas and Kwan, 2017).

Contrary to the classical view of motor cortex as entirely agranular, high-resolution mapping reveals a narrow yet distinct, densely packed granular layer 4 (L4) spanning across MOp and MOs Integrating cytoarchitecture with retrograde and anterograde connectivity parcellates MOp-ul into 11 distinct layers and sublayers (1, 2, 3, 4, 5a, 5b-superficial, 5b-middle, 5b-deep, 6a-superficial, 6a-deep, and 6b) housing 26 discrete projection neuron (PN) subtypes. These fall into three broad classes: 16 intratelencephalically (IT) types distributed from L2 to L6b (including L4 neurons targeting MOs/SSp, L2/L5 neurons projecting to the temporal association area, and distinct L5a versus L5b subsets that differentially innervate the striatum), 7 extra telencephalic/pyramidal tract (ET/PT) types restricted to L5 that project down to the brainstem and spinal cord, and 3 corticothalamic (CT) types localized in L6 that provide reciprocal feedback to the thalamus (R. Munoz-Castenada et al., 2021).

2.2 Caudate Nucleus And The Putamen: Gross Morphology And Cellular Organization

Anatomically, the striatum divides into the ventral striatum, comprising the nucleus accumbens and olfactory tubercle, and the dorsal striatum, consisting mainly of the caudate nucleus and the putamen. The mouse dorsal striatum, also known as the caudate-putamen (CP), differs structurally from its human counterpart by remaining a solid, unified mass stretching along the rostrocaudal axis beneath the cerebral cortex, rather than being split into two separate structures (Fig.11). While its tissue lacks the layered lamination found in other areas of the telencephalon, its signature striped appearance is driven by the unique coexistence of striosomes and a surrounding matrix. As a core component of basal ganglia circuits, the caudate-putamen integrates a vast array of information vital for motor control, cognition, and emotion. It receives heavy input from both telencephalic regions, primarily the cerebral cortex and the thalamus, and non-telencephalic areas. Among the latter, the nigrostriatal pathway running from the substantia nigra to the striatum holds massive medical relevance; when these nerve fibers degenerate, it directly drives the characteristic reduction in motor activity seen in Parkinson's disease. Furthermore, it is also involved as a central hub in cortico-cortical loops.

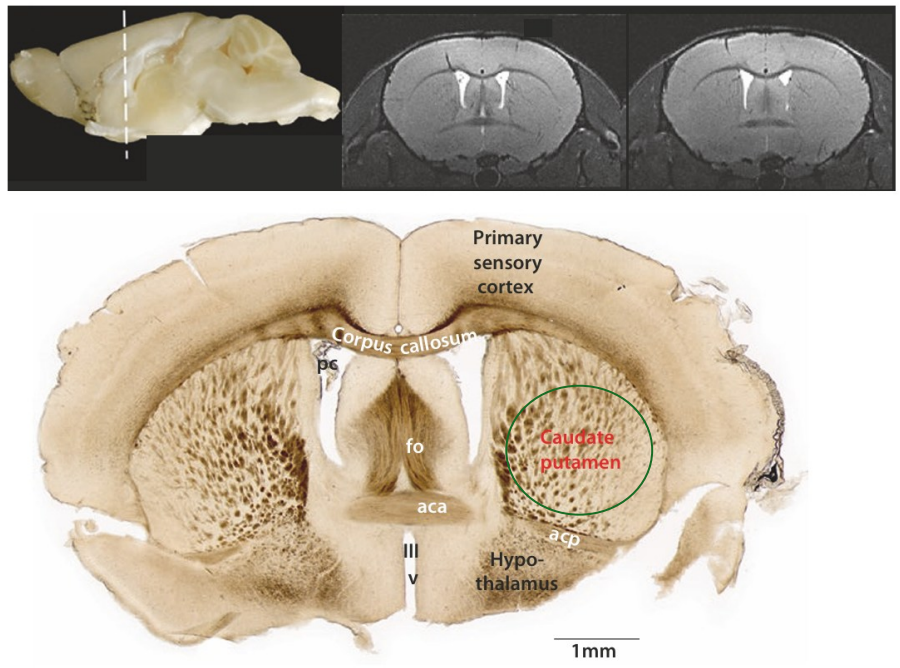


Figure 11. Coronal section of mouse brain, where it is possible to visualize the caudate-putamen (image adapted from Schröder et al., 2020).

2.2.1 Microscopical organization

The CP complex looks uniform and lacks the distinct layering found in the nearby cerebral cortex. Despite this uniform appearance, its internal structure is far from simple, living up to the classic name striatum, or corpus striatum, with a distinctly striped texture under both macro and microscopic inspection. Looking closer reveals that this striped pattern actually comes from two different regions: a matrix and the striosomes. Over 90 percent of all striatal neurons consist of GABAergic medium spiny neurons, also called striatal projection neurons, expressing D1 or the D2 dopamine receptors (Petryszyn et al. 2017), which integrate glutamatergic signals originating in the cerebral cortex and thalamus. These projection neurons respond with episodic bursts of spike activity that result in transient disinhibition of basal ganglia targets like the thalamus, split roughly evenly between striatonigral and striatopallidal pathways. Beyond these projection neurons, the mouse striatum houses several distinct types of GABAergic interneurons defined by unique transmitter profiles and electrophysiological properties: parvalbumin-containing interneurons drive feedforward inhibition to regulate spike timing in projection neurons, receiving inputs primarily from the cortex and thalamus while projecting locally to both direct and indirect pathway neurons; somatostatin, neuropeptide Y, and nitric oxide synthase-containing interneurons feature unique persistent depolarizing plateau potentials and low-

threshold spikes, possessing the rare ability among neurons to branch into two separate individual axons; calretinin-positive interneurons remain the least understood group, identified primarily through immunohistochemistry in three distinct morphological forms despite a current lack of electrophysiological data; tyrosine hydroxylase-positive interneurons feature dense axonal collateral plexuses with at least four distinct electrophysiological profiles (Tepper et al. 2010), receiving excitatory inputs from cortical sources and inhibitory inputs from projection neurons. Meanwhile, cholinergic interneurons represent the largest interneuron group and stand out as the sole non-GABAergic interneurons in the structure, exciting local GABAergic interneurons that subsequently inhibit projection neurons (Faust et al. 2016).

2.2.2 Caudate Putamen circuitry

The CP serves as a central hub within the basal nuclei, which in mammals generally comprise the striatum, globus pallidus (known as the entopeduncular nucleus in rodents), substantia nigra, and subthalamic nucleus. Functionally, these structures process information through largely nonoverlapping loops linking some regions of the cortex, the basal ganglia, and the thalamus (Kreitzer and Malenka, 2008; Pan et al., 2010) (Fig.12). A study reveals a vast array of projections to the mouse striatum, originating from the deep layers of frontal and parietal cerebral cortices, various thalamic nuclei, the basolateral and central amygdala, and brainstem centers such as the substantia nigra pars compacta, ventral tegmental area, retrorubral field, and raphe nuclei (Pan et al., 2010).

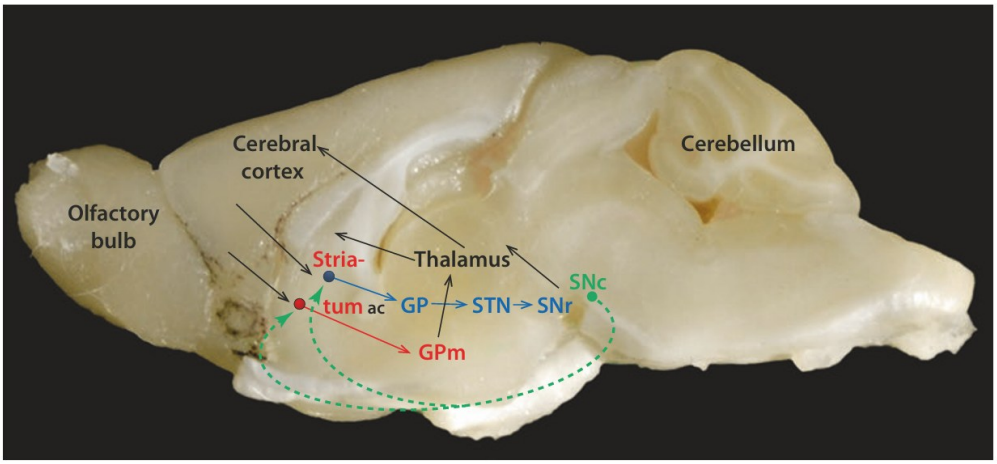


Figure 12. Schematic representation of the main connectivity of the CP/striatum (image adapted from Schröder et al., 2020)

Functionally and clinically, the striatum drives two major output pathways under cortical control and dopaminergic modulation from the substantia nigra pars compacta (SNc), which supplies the nigrostriatal tract (Zeiss, 2005). These dopaminergic fibers synapse onto two distinct populations of

GABAergic medium spiny neurons (MSNs) within the striatum: one expressing D1 dopamine receptors and the other expressing D2 receptors, subtypes that differ pharmacologically, with dopamine exciting D1 and inhibiting D2 synapses (Planert et al., 2013). D1 MSNs initiate the direct striatonigral pathway, projecting to the medial globus pallidus and the substantia nigra pars reticulata to yield a net inhibitory output. Conversely, D2 MSNs form the indirect pathway, first relaying through the globus pallidus to the subthalamic nucleus (Loucif et al., 2005), which then contacts the medial globus pallidus and substantia nigra pars reticulata to produce a net excitatory output. The loop is completed as axons from the substantia nigra pars reticulata project to ventromedial thalamic motor nuclei, which receive balanced inhibitory and excitatory input before sending glutamatergic projections back to the cortex.

2.3 The Cerebellum

The cerebellum, which means *little brain* in Latin, is the oldest part of the suprasegmental brain. It first developed alongside the balance system in fish. While it stayed very basic in crawling animals like amphibians and reptiles, it grew significantly as animals started walking on four legs and, eventually, stood upright on two (Schröder et al., 2020). Even though its cortex has a simple three-layer design with a uniform structure, the cerebellum holds about half of all the neurons in the vertebrate brain. Rather than following strict animal classifications, its size and complexity depend on the physical skills an animal needs to survive. Over time, its growing connections with the motor cortex, the balance system, and the spinal cord clearly show how important it is for coordinating and learning movements (FitzGerald 2015). In mice, the cerebellum sits at the back and top of the skull. The cranial bones that surround it are the parietal bone on top, the occipital bone at the back, and both the occipital and interparietal bones on the sides. Finally, a layer of tough tissue called the *tentorium cerebelli* separates the sides of the cerebellum from the occipital lobes of the cerebrum (Klintworth 1968).

2.3.1 Anatomy of the cerebellum

Topographically, the mouse cerebellum anchors the dorsocaudal pole of the brain. When viewed in midsagittal profile, its rostral surface directly leans on the mesencephalic quadrigeminal plate while its ventral aspect interfaces with the brainstem and roofs the fourth ventricle (Fig. 13) (Schröder et al., 2020).

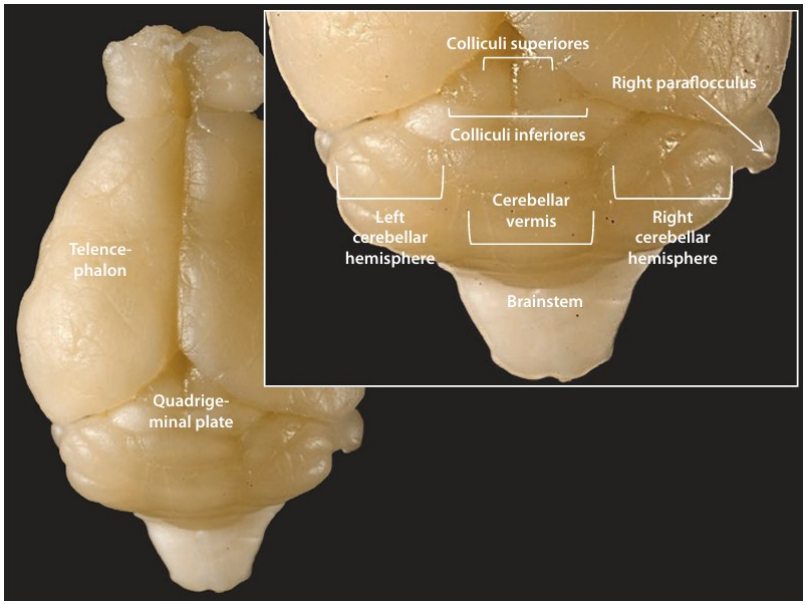


Figure 13. Dorsal view of the mouse brain with the point of attachment of the cerebellum (image adapted from Schröder et al., 2020).

In a midsagittal cut, the macroscopic branching of cerebellar white and gray matter evokes the silhouette of a miniature tree, a configuration classically designated as the *arbor vitae*. (Fig. 14) (Schröder et al., 2020). From a dorsal perspective, the murine cerebellum conforms to the standard mammalian architectural blueprint: a central median strip known as the *vermis* flanked on either side by the cerebellar hemispheres. Along the anteroposterior axis, the vermal surface is characterized not by smooth tissue, but by a series of tight transverse ridges or folds known as folia; by increasing the overall surface area of the cortex, the extensive foliation of the cerebellum allows for the integration of a vastly higher number of neurons compared to a smooth, non-foliated structure (Van Essen, 2002). Developmentally, the *vermis* can be traced back to five embryonic lobes which consolidate by adulthood into three definitive primary lobes: the anterobasal and anterodorsal lobes merge to form the anterior lobe, the central and posterior divisions coalesce into the posterior lobe and the nodulus and flocculus combine to establish the flocculonodular lobe (Fig. 15) (Schröder et al., 2020).

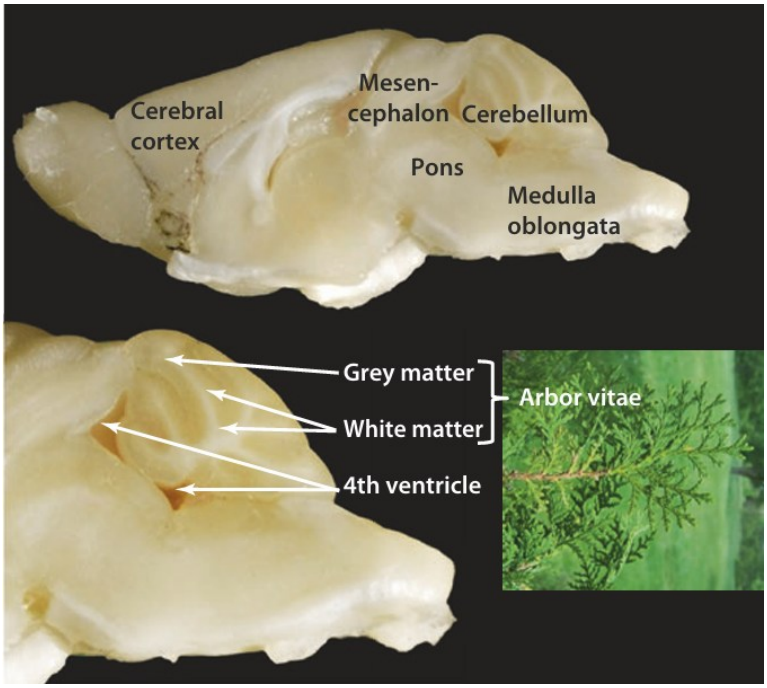


Figure 14. Median section of the mouse brain displaying cerebellar anatomical boundaries (left to right: midbrain, pons, and medulla oblongata) and the arbor vitae architecture, formed by deep white matter tracts bordered by cerebellar gray matter. (Image adapted from Schröder et al., 2020).

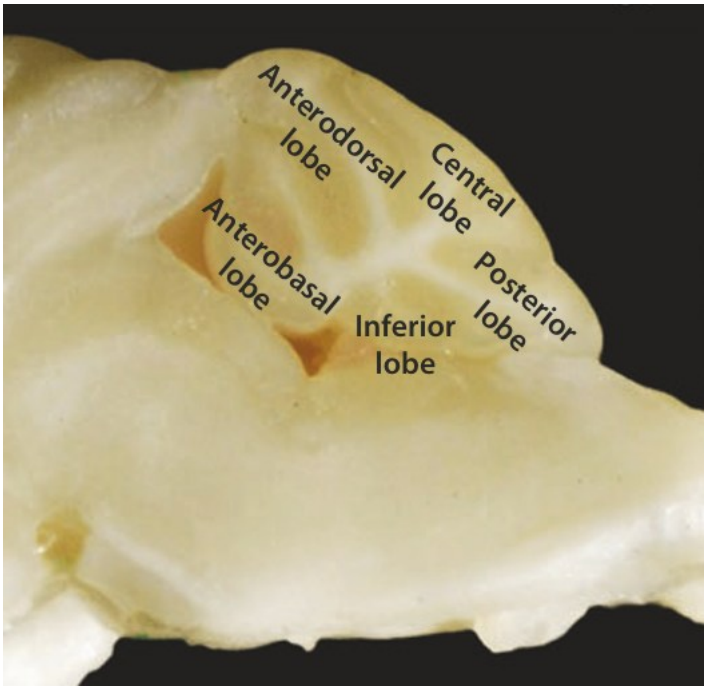


Figure 15. Midsagittal section of the mouse brain showing the different cerebellar lobes (Image adapted from Schröder et al., 2020).

Structurally, the cerebellum comprises an outer gray matter mantle and an inner white matter core. The gray matter forms the three-layered cerebellar cortex, enveloped on its external surface by the cranial meninges (Schröder et al., 2020). Beneath the cortex lies the centrally situated white matter, the *corpus medullare cerebelli*, which roofs the fourth ventricle ventrally, houses the highly vascularized choroid plexus adjacent to the caudal vermis, and exhibits the characteristic branching pattern known in sagittal profile as the *arbor vitae*. Embedded bilaterally within this white matter core are the deep cerebellar nuclei, which generate the primary output pathways of the cerebellum to downstream brain targets: (i) the dentate nucleus, (2) the fastigial nucleus, and (iii) the interposed nucleus, the latter comprising the emboliform and globose nuclei (Schröder et al., 2020).

2.3.2 Cerebellar cortex

At the histological level (Fig.16), the distinctive architecture of the cerebellar *vermis* becomes readily apparent: the arborizing white matter core is enveloped by the more darkly Nissl-stained cerebellar cortex (Schröder et al., 2020). Higher magnification reveals the centrally situated white matter bordered by the granular layer, densely packed with small somas, and the sparsely populated molecular layer (ML). Between these two zones lies the mono-layered Purkinje cells stratum, identifiable by its large perikaryal (Schröder et al., 2020). The molecular layer is bounded externally by the cranial pia mater.

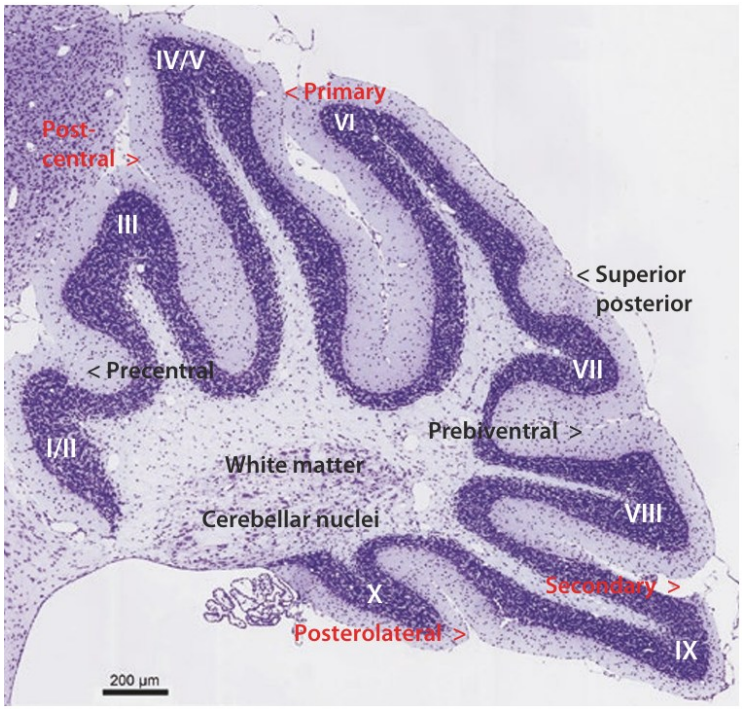


Figure 16. Parasagittal paraffin section of a mouse brain stained with Nissl, indicating the names of the cerebellar lobules (image adapted from, Schröder et al., 2020, a courtesy of: Dr. Christoph Köhler, Maia Dinekov)

I-Molecular layer

Beyond its dense neuropil of fibers, the molecular layer hosts two distinct populations of inhibitory interneurons, basket cells and stellate cells, segregated along a depth-dependent spatial gradient. Basket cells predominantly populate the deep half of the ML, whereas stellate cells are concentrated within the upper, more superficial zone (Fahrion et al. 2013).

Although both cell types target Purkinje cells, their synaptic architectures diverge significantly (Ango et al. 2008). Basket cells feature rounded somata (approximately 10 µm in diameter) that give rise to a planar dendritic arbor spanning 180° through the ML; their smooth axons travel parallel to the PC layer, projecting collaterals that wrap the axon initial segments of multiple Purkinje cells in characteristic basket-like pericellular nests (Ango et al. 2008). In contrast, stellate cells possess small cell bodies (8–12 µm across) with sparse, modestly branched dendrites restricted to the outer ML. Rather than targeting the perisomatic domain or initial segment, their axons project toward Purkinje cells to establish synapses directly along the PC dendritic arborizations (Barmack and Yakhnitsa, 2008).

The adult murine ML is further characterized by Bergmann glia, a specialized cerebellar astroglial subtype consisting of ascending radial processes derived from Golgi epithelial cells (distinct from cerebellar Golgi interneurons). Positioned at the boundary zone between the Purkinje and granular

cell layers (GCLs), these glial somata project vertical shafts across the entire depth of the ML. At the pial surface, the expanded endfeet of these fibers coalesce to build the outer *glia limitans*, forming an intimate structural interface with the cranial pia mater (Cheng et al., 2018).

II-Purkinje cell layer

PCs are large neurons with cell bodies about 40 μm in diameter, arranged in single layer in the adult mouse. Each PC sends out a thin, myelinated axon that travels down into the white matter to connect with the deep cerebellar nuclei. In the opposite direction, the dendritic trees of the PCs extend upward and branch into the ML, where they make synaptic contact with about 150,000 parallel fibers (Harvey and Napper, 1991).

In sagittal sections of the adult mouse cerebellar cortex, these dendritic trees look wide, dense, and highly branched; in contrast, when viewed in coronal sections, they appear thin and flat (Adkins-Regan 1997).

III-Internal granular layer

Granule cells can be identified by their location in the granular layer, below the PCs layer, their small cell bodies (about 6–8 μm in diameter), and their claw-shaped dendrites (Barmack and Yakhnitsa 2008). They receive excitatory input from mossy fibers and send their axons up into the ML. There, these axons split in a T-shape and lose their myelin sheath to form the parallel fiber system, which makes synaptic contacts with PC dendrites (Schröder et al., 2020). Golgi cells are found inside the granular layer; they make up about two-thirds of all cerebellar GABAergic interneurons and provide the only inhibitory input to granule cells (Cesana et al. 2013). The axon terminals of Golgi cells and the dendrites of granule cells meet around mossy fibers to form a synaptic structure called the cerebellar glomerulus. Through a negative feedback loop, this structure helps control the spike patterns of PCs (D'Angelo et al. 2013). Golgi cells have large, polygonal cell bodies (10–20 μm in diameter) and wide-branching axon terminals; their dendrites grow toward the pial surface and enter the ML (Barmack and Yakhnitsa 2008). Finally, the granular layer contains unipolar brush cells (UBCs). Together with granule cells, UBCs are the only glutamatergic excitatory interneurons in the cerebellar cortex. They have cup-shaped cell bodies (8–10 μm in diameter) and a single dendrite that ends in a group of short branches (Barmack and Yakhnitsa 2008). Each UBC receives input from one mossy fiber that brings in vestibular signals, forming a very large synapse across the entire dendritic brush; the axons of UBCs then project mostly to granule cells (Schilling et al. 2008).

2.3.3 Cerebellar neural circuits

Cerebellar wiring divides broadly into two organizational systems: an extrinsic network of afferent and efferent projections, and an intrinsic network governed by local interneurons (White and Sillitoe 2013) (Fig.17). All incoming sensory and motor signals arise from precerebellar nuclei, a heterogeneous collection of medullary and spinal centers, and ultimately funnel toward cerebellar PCs (Fu et al. 2011). Excitatory input reaches the cortex through two distinct fiber systems: climbing fibers, each originating from the inferior olivary complex to make direct, powerful contacts with both the soma and dendritic tree of an individual Purkinje cell (Xiao and Scheiffele 2018), and mossy fibers, which emerge from brainstem precerebellar nuclei (such as the pontine nuclei) and ascending spinal tracts to deliver sensorimotor signals. Instead of contacting PCs directly, mossy fibers synapse onto granule cells, whose axons ascend into the ML to form the parallel fiber network and provide widespread excitatory input to Purkinje dendrites. Purkinje cells then generate the sole efferent output of the cerebellar cortex, sending inhibitory, GABAergic projections down to the deep cerebellar nuclei embedded in the white matter; these deep nuclei, modulated entirely by PC inhibition, supply the main cerebellar output to motor targets across the central nervous system, including the red nucleus and the motor nuclei of the dorsal thalamus (Schröder et al., 2020)

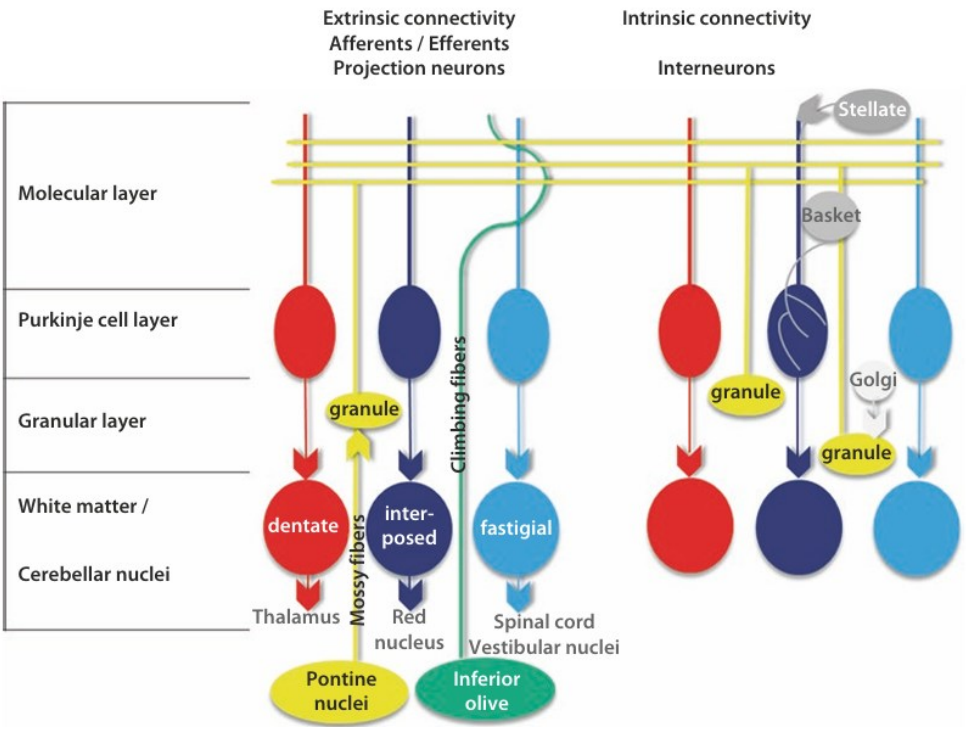


Figure 17. Schematic representation of the extrinsic and intrinsic connectivity of the cerebellum (image adapted from Schröder et al., 2020).

2.3.4 Higher cognitive and motor functions of the cerebellum

Descending corticospinal tract (CST) axons in the mouse directly synapse onto proprioceptive afferents that target dorsal spinocerebellar neurons in Clarke's column (Hantman and Jessell 2010). Through this arrangement, the CST tunes incoming proprioceptive signals en route to the cerebellum well before reaching ventral horn motoneurons, adjusting sensory feedback to match the planned motor command. In parallel, the motor cortex communicates with the cerebellum through a descending cerebro-cerebellar route: cortical efferents innervate the pontine nuclei, which project via the ponto-cerebellar tract to reach cerebellar Purkinje cells through the mossy fiber-parallel fiber system. This cortico-cerebellar-cortical loop is closed by the ascending dentato-rubro-thalamic pathway, in which efferents from the deep cerebellar nuclei, primarily the dentate nucleus, cross the midline to target the red nucleus and the ventral lateral (VL) nucleus of the thalamus. Acting as an integrative motor hub that also receives cortical and striatal inputs, the VL nucleus sends reciprocal projections back to the primary motor cortex. (Tlamsa and Brumberg 2010).

Beyond its canonical role in coordinating movement, posture, and equilibrium, the cerebellum critically modulates non-motor cognitive and affective domains, including working memory, language

processing, and emotional regulation (Jacobi et al. 2021). In clinical contexts, structural and functional cerebellar deficits can precipitate emotional dysregulation and anxiety-related disorders, hallmarks of cerebellar cognitive affective syndrome (Argyropoulos et al. 2020). Many of these behavioral alterations trace directly to cerebellar vermis dysfunction (Grossauer et al. 2015), as experimental lesions targeting this region disrupt defense behaviors triggered by salient emotional stimuli (Utz et al. 2015). Cerebellar organization relies on functional modules defined by discrete olivo-cortico-nuclear loops. The vermis constitutes the core of "module A": its parasagittal cortical stripe receives climbing fiber input from the caudal medial accessory olive, while its PCs deliver inhibitory output to the medial subnucleus of the fastigial nucleus (Apps and Hawkes 2009). The fastigial nucleus, in turn, projects broadly across subcortical and forebrain centers, including the periaqueductal gray (PAG), amygdala, hypothalamus, dorsal striatum, hippocampus, and prefrontal and parietal cortices (Heath and Harper 1974). Because emotional responses integrate cognitive, somatomotor, and autonomic drives, distinct subregions or micromodules within module A are thought to coordinate specific facets of affective processing. Extensive vermal lesions spanning lobules III–VIII blunt fear- and anxiety-related defensive reactions in rodents exposed to anxiogenic contexts (Apps et al., 2018). Within the posterior vermis: (i) lobules VI and VII direct head orientation and saccadic eye movements across mammalian species (Takagi et al., 2000); (ii) lobule VIII mediates innate and conditioned fear-evoked freezing without perturbing baseline locomotor performance (Koutsikou et al., 2014); (iii) lobules IX and X modulate autonomic outflow, including blood pressure, heart rate, respiration, and the baroreceptor reflex (Apps et al., 2018).

3 AIM OF THE STUDY

Developed in the last decades, new synthetic cannabinoids are potent psychoactive substances; they act primarily as cannabinoid receptors full agonists and can induce marked psychiatric and physical adverse effects including altered cognitive functions and locomotor activity (Bilel et al., 2023; Corli et al., 2024). Among them, JWH-018 is a widely studied synthetic cannabinoid: previous *in vivo* and *in vitro* electrophysiological studies have demonstrated that JWH-018 preparations negatively impact memory retention in the hippocampus; in mice, both acute and repeated exposure to this drug has been associated with behavioural and neuroadaptive changes of the endocannabinoid and dopaminergic systems (Corli et al., 2026; Barbieri et al., 2016). Building on this, the aim of the present thesis work was to further investigate the neurobiological effects induced by exposure to the synthetic cannabinoid JWH-018 in a murine model, focusing on core CNS motor structures (i.e., the motor cortex, dorsal striatum, and cerebellum). Particular attention was paid to potential morphological alterations and changes in calcium homeostasis, as a functional readout of overall cellular homeostasis across these brain regions. Given the role of cannabinoid signalling in the regulation of neuronal activity, including intracellular calcium dynamics, this study integrated a morphological assessment of tissue architecture with immunohistochemical profiling of three canonical calcium-binding proteins, parvalbumin, calbindin, and calretinin, to investigate potential changes in neuronal Ca^{2+}-buffering systems across the selected brain regions.

4 MATERIAL AND METHODS

This research project was conducted within a multicenter framework that brought together the Laboratory of Cellular Biology and Neurobiology (Department of Biology and Biotechnology "L. Spallanzani"), the Clinical and Experimental Toxicology Laboratory (Toxicology Unit, Poison Control Center, CNIT – Istituti Clinici Scientifici Maugeri SpA, IRCCS Pavia), and the Forensic Toxicology Laboratory (Legal Medicine, LTTA Center – Department of Morphology, Surgery and Experimental Medicine, University of Ferrara). The experimental synergy was fostered by Prof. Matteo Marti as part of the project "Effects of NPS: Development of a Multicenter Study to Strengthen the Early Warning System," funded in collaboration with the Anti-Drug Policies Department (DPA) of the Italian Presidency of the Council of Ministers.

This study was conducted in accordance with Italian legislation governing experimental research protocols (Legislative Decree 116/92) and the European Directive 2010/63/EU on the protection of animals used for scientific purposes. The experimental procedures also adhered to the guidelines established by the institutional animal welfare body, as well as the Ethics Committees of the University of Pavia and the University of Ferrara. All animals were handled humanely pursuant to institutional guidelines, with every effort made to minimize both animal suffering and the number of subjects used.

4.1 Animals

Experiments were conducted on male ICR (CD-1®) mice aged 3–4 months (body weight: 25–30 g), supplied by ENVIGO Harlan Italy and bred at the Laboratory for Preclinical Research (LARP), University of Ferrara. Mice were housed in groups of five per cage (80 cm^2/animal floor space, 12 cm minimum height) under standard environmental conditions: 20–22 °C, 45–55% relative humidity, and an inverted 12:12 h light/dark cycle (lights on at 06:30). Standard chow (Diet 4RF25 GLP; Mucedola, Milan, Italy) and tap water were available *ad libitum*.

4.2 Drug Preparation And Doses Choice

JWH-018 was obtained from LGC Standards (LGC Standards s.r.l., Milan, Italy). Each compound was preliminarily solubilized in a vehicle mixture consisting of 5% absolute ethanol (BioUltra, molecular biology grade, ≥99.8%; Sigma-Aldrich, Milan, Italy) and 2% Tween 80 (Sigma-Aldrich, Milan, Italy), then diluted to the final working volume with physiological saline (0.9% NaCl; Eurospital, Trieste, Italy). The solution made with ethanol, Tween 80 and saline was used as the vehicle.

4.3 Experimental Design

Animals were randomly allocated into two experimental groups: (i) treated control animals and (ii) JWH-018-treated mice. Animals in the treated group received daily intraperitoneal (i.p.) injections of JWH-018 at a dose of 6 mg/kg once a day for seven consecutive days. Control animals were administered an equivalent volume of vehicle (0,004 ml/kg, i.p.) following the same temporal administration schedule. For histological and immunohistochemical analyses, randomly selected mice were sacrificed 24 hours following the final injection (day 8) to investigate the short-term cumulative effects of repeated JWH-018 administration versus vehicle exposure across days 1 to 7. Central nervous system tissues were collected and processed for further histological and immunohistochemical analyses.

4.4 Tissue Preparation

Following euthanasia via cervical dislocation, whole brains were promptly excised according to established protocols and washed with saline (0.9% NaCl) solution. Tissue fixation was carried out by immersion in 4% paraformaldehyde in 0.1 M phosphate buffer (pH 7.4) for 24h at room temperature. Subsequently, samples were dehydrated in absolute ethanol for 1 h, cleared in acetone, and finally embedded in Paraplast X-TRA (Sigma-Aldrich, Milan, Italy). Serial sectioning was performed on a manual rotary microtome, generating 8-µm-thick sagittal slices for both the cerebral hemispheres and the cerebellar vermis. Sections were mounted onto silane-treated slides for subsequent histochemical and immunohistochemical assessments.

4.5 Hematoxylin And Eosin

Hematoxylin and eosin (H&E) staining remains the gold-standard histological method for assessing tissue architecture and pathological alterations (Fischer et al., 2008). In this bipartite staining system, oxidized hematoxylin acts as a basic dye with high affinity for polyanionic cellular structures, primarily nuclear chromatin and nucleic acids, staining them deep blue-violet. Conversely, eosin is an acidic counterstain that binds positively charged amino groups in cytoplasmic proteins and extracellular matrix components, imparting variable shades of pink to red (Martini et al., 2016; Santos Ferreira, 2003). Paraffin-embedded sections were first deparaffinized in xylene and progressively rehydrated through a graded ethanol series to water. Specimens were stained with Carazzi's hematoxylin for 10 min at room temperature, thoroughly rinsed under running tap water for 20 min, and briefly counterstained with eosin (1–2 s). Following consecutive rinses in distilled water and 80% ethanol, slides were fully dehydrated through ascending ethanol grades, cleared, and coverslipped using Eukitt mounting medium (Kindler GmbH, Freiburg, Germany). Bright-field histological observations were conducted

with an Olympus BX51 optical microscope (Olympus, Tokyo, Japan), and representative microphotographs were captured using an Olympus EP50 (Olympus Italia, Segrate, MI, Italy).

4.6 Immunohistochemical Reactions

To evaluate the expression and regional distribution of the calcium-binding proteins parvalbumin (PV), calbindin (CALB1), and calretinin (CR), immunohistochemical staining was performed on murine brain sections using commercially available antibodies. Cerebral and cerebellar sections were first deparaffinized in xylene and gradually rehydrated through graded ethanol solutions. After blocking endogenous peroxidases and non-specific sites, tissue slices were incubated overnight at 4 °C in a humid chamber with the appropriate commercial monoclonal primary antibodies (Table 2). Antigen–antibody binding was detected by incubating slices for 30 min with a specific biotinylated secondary antibody and processing them with the Vectastain Elite ABC Kit (Vector Laboratories, Burlingame, CA, USA) according to the avidin–biotin–peroxidase method. The chromogenic reaction was developed using 3,3′-diaminobenzidine tetrahydrochloride (DAB; Sigma-Aldrich, St. Louis, MO, USA) as chromogen. Sections were then counterstained with Carazzi's hematoxylin for 30s, dehydrated in graded ethanol solutions, cleared in xylene, and mounted with Eukitt (Kindler GmbH, Freiburg, Germany). To assess antibody specificity, sections processed without the primary antibody were used as negative controls; no immunoreactivity was observed in these tissues. Finally, slides were examined under bright-field microscopy using an Olympus BX51 optical microscope (Olympus, Tokyo, Japan) and the images were acquired with an Olympus EP50 (Olympus Italia, Segrate, MI, Italy.

Primary antibodies	Species	RRID code	Manufacturer, Mono-Polyclonal and Cat. No.	Dilution
Anti-calretinin	Rabbit	AB_2228331	Sysy Antibodies, Gottingen, Germany, Polyclonal, Cat# 214 102	1:200
Anti-parvalbumin	Rabbit	AB_2156474	Sysy Antibodies, Gottingen, Germany, Polyclonal, Cat# 195 002	1:500
Anti-calbindin	Mouse	AB_2068201	Sysy Antibodies, Gottingen, Germany, Polyclonal, Cat# 214 011	1:500
Secondary antibody				
Anti-rabbit	Goat	AB_2916034	Vector Laboratories, Burlingame, CA, USA, Polyclonal, Cat# PI-1000-1	1:200
Anti-mouse	Horse	AB_2336821	Vector Laboratores, Burlingame, CA, USA, Cat# PK-6102	1:200

Table 2. Antibodies utilized for immunohistochemical reactions.

4.7 Quantitative Analysis: Optical Density

Immunohistochemical and histological staining were performed on sagittal sections of the cerebellar vermis and forebrain (6 slides per mouse, 4 sections per slide) obtained from treated ($n = 2$) and control ($n = 2$, Ctrl) mice. Microscopic examination and quantitative analyses were carried out on 4 sections per slide, focusing on the neocerebellar lobules within the cerebellum, as well as the primary motor cortex and dorsal striatum within the cerebrum. Findings from treated animals were subsequently compared against those of the control group. Densitometric analysis was carried out using ImageJ software (version 1.48i): grayscale images were obtained and subsequently inverted, rendering immunopositive regions brighter than the unstained background. Signal intensity was evaluated as optical density (OD, mean pixel value) across immunoreactive regions. Specifically, to quantify Calbindin signal intensity exclusively within the soma of PCs, regions of interest (ROIs) were outlined using the "polygon section" tool (Fig.18), adjusting the dimensions to fit individual cell body diameters; at the level of the caudate-putamen and the primary motor cortex, the ‘polygon section’ tool was used for manual tracing of the cellular bodies and axons.

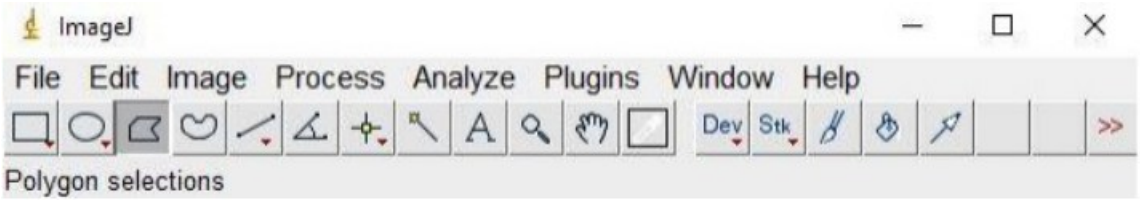


Figure 18. Regions of interest (ROIs) were manually delineated using the Polygon selection tool from the ImageJ toolbar.

Across all analyses, ROI geometric parameters (circles, ellipses, and polygons), image magnification, and the number of measurements were kept strictly constant. Immunocytochemical intensity, expressed as optical density, was quantified in a double-blind manner across 3 randomized fields per section (performing at least 10 measurements per image) on 4 sections per animal for each experimental group. Raw data were subsequently compiled in Microsoft Excel for preliminary organization.

4.8 Statistical Analysis

Densitometric data were processed using Microsoft Excel to determine: (i) the mean value of 12 measurements per analyzed image, (ii) the average OD across the 3 images per treatment in both experimental groups, and (iii) the corresponding standard error of the mean (SEM). Final data were expressed as mean ± SEM and presented as histograms. Statistical differences between control and treated groups were evaluated using an unpaired Student's t-test for normally distributed data and Mann Whitney for non-normally distributed data (GraphPad Prism Software, lnc). Thresholds for statistical significance were set as follows: significant at $p < 0.05$ (*), very significant at $p < 0.01$ (**), and extremely significant at $p < 0.001$ (***); values with $p > 0.05$ were considered not statistically significant.

5 RESULTS

5.1 Gross Morphology

Routine hematoxylin and eosin (H&E) staining represents the fundamental gold standard for the cytoarchitectural and morphological analysis of biological tissues (Fischer et al., 2008). This dichromatic approach relies on the differential binding affinity of two dyes toward subcellular components: hematoxylin, a basic dye, selectively binds to negatively charged (basophilic) structures such as nucleic acids, imparting a characteristic blue-purple hue to cell nuclei; conversely, eosin, an acidic dye, targets cationic (acidophilic/eosinophilic) components within the cytoplasm and the extracellular matrix, staining them in varying shades of pink (Fischer et al., 2008). In the present study, H&E staining was employed as a preliminary qualitative and quantitative screening tool to characterize structural tissue integrity and to identify potential histopathological alterations across the three investigated areas of interest: MOp, CP and CRBL. Specifically, this analysis enabled the systematic evaluation of cytoarchitectural organization, including cell polarity preservation, layer thickness, and structural continuity specific to each region, as well as nuclear and cellular alterations or hallmarks of cell suffering and death (apoptosis/necrosis), alongside the assessment of inflammatory infiltrates and stromal remodeling evident through changes in interstitial matrix density and arrangement (Cardiff et al., 2014). Histological examination using hematoxylin and eosin staining revealed morphological alterations in animals treated with JWH-018 (6 $mg \cdot kg^{-1}$) (e-j) compared to vehicle (a-d) across all examined brain areas (Fig.19). In vehicle, the morphological cytoarchitecture of the mouse brain was well preserved in all the investigated areas, with (i) the primary motor cortex (MOp) and (ii) striatum (Fig. 19, panels a, b, c) showing a compact and continuous neuropil with physiological cellular morphology and organization, as well as (iii) the cerebellum (panel d), exhibiting an intact trilaminar cytoarchitecture with an organized and uncompromised white matter region. In contrast, exposure to JWH-018 induced widespread parenchymal and microvascular damage throughout the forebrain and cerebellum. Specifically, both the MOp (panels e, h) and the striatum (panels f, i) showed pronounced parenchymal vacuolization, visible as optically empty spaces, accompanied by the presence of intraparenchymal hemorrhagic foci. In parallel, the cerebellum of treated animals (g, j) displayed localized extravasations of red blood cells primarily within the cerebellar medullary white matter. Collectively, these pathological hallmarks of excitotoxicity-like neurodegeneration and vascular compromise provided the morphological rationale to further investigate dysregulations in intracellular calcium signaling pathways.

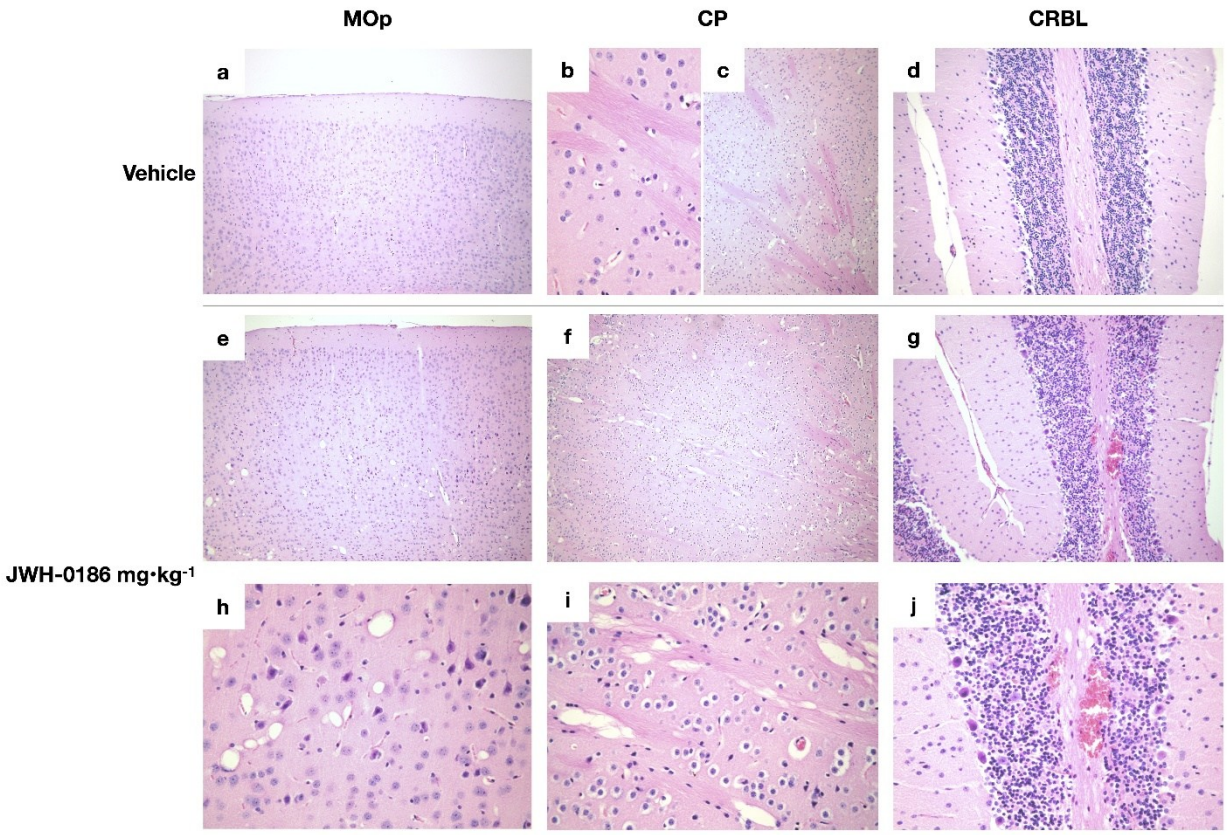


Figure 19. Hematoxylin & Eosin staining of MOp. CP and CRBL of either vehicles (a-d) or JWH-018 (6mgxkg-1) treated animals (e-j).

5.2 Immunohistochemistry

In this work, parvalbumin, calretinin and calbindin were assessed as complementary calcium-binding proteins, providing a readout of potential alterations in neuronal Ca^{2+} buffering in response to JWH018-mediated cannabinoid signaling. These proteins are expressed by different cellular populations, with distinct distributions and functions; therefore their combination allows a broader characterization of neuronal populations (CW Heizmann, 1993). Given the role of the cannabinoid system in the regulation of neuronal activity and synaptic functions, in this study we employed immunohistochemical reactions for PV, CR and CALB1 to investigate whether JWH018 exposure is associated with changes in neuronal calcium-binding profiles in different brain motor areas, i.e the primary motor cortex, the striatum and the cerebellum.

Parvalbumin

Parvalbumin is a small (11–12 kDa, 106–113 amino acids), cytosolic, water-soluble Ca2+-binding protein that freely fills neuronal somata, nuclei, axons, and dendrites. Immunocytochemistry in the neocortex reveals intense immunoreactivity in cell bodies and nuclei compared to neuronal processes, alongside associations with microtubules, postsynaptic densities, and intracellular membranes (Stichel CC et al., 1987; Schwaller B., 2010). At the network level, PV-expressing (PV+) GABAergic neurons represent the largest subpopulation of neocortical interneurons, accounting for roughly 40% of the total population, and critically modulate the activity of projection pyramidal neurons (Tremblay R. et al., 2016). Overall, PV immunohistochemical staining showed comparable differences between JWH-018- and vehicle-treated animals in all brain areas under investigation, although the immunopositivity appears fainter in the former. Particularly, in the primary motor cortex and caudate-putamen PV immunopositive cells could be clearly identified showing discrete immunopositive neuronal somata distributed throughout the cortical layers and dorsal striatum, accompanied by PV-positive neuronal processes. Parallelly, in the cerebellum strong and widespread PV immunopositive cells were strictly localized in the molecular layer of both experimental groups, although the signal appeared more evident in control mice. In addition, sparse Purkinje cells showed weaker immunopositivity, particularly visible in vehicle-treated samples. The quantitative analysis revealed that the PV immunoreactive optical density was significantly decreased in both the motor cortex and dorsal striatum following JWH-018 administration (6 mg/kg) (Fig.20, panels A-B). Similarly, quantitative assessments at the level of Purkinje cell somata showed a significant reduction in treated animals (Fig.20 panel C) whereas a slight increase in PV optical density was observed in treated animals within the molecular layer of the cerebellum (Fig.20, panels D). Specifically, within the primary motor cortex (Fig. 20A), a statistically significant decrease in PV immunoreactivity was observed in layer 5 of treated mice compared to vehicle (96.23 ± 2.58 and 116.38 ± 1.59, for JWH-018-treated mice and vehicle respectively). Within the caudate-putamen region, the decrease in OD observed in cells from treated animals remained statistically significant compared to vehicle (101.35 ± 6.92 and 120.25 ± 3.40, for JWH-018-treated mice and vehicle respectively); the reduction in OD measured in Purkinje cells was also statistically significant in the treated group, compared to vehicle (126.51 ± 1.84 and 148.81 ± 1.82, for JWH-018-treated mice and vehicle respectively). Conversely, this pattern was reversed only in the molecular layer of the cerebellum, which exhibited a slight, barely significant increase in OD in treated animals, compared to vehicle (173.25 ± 2.79 e 167.39 ± 2.19, for JWH-018-treated mice and vehicle respectively).

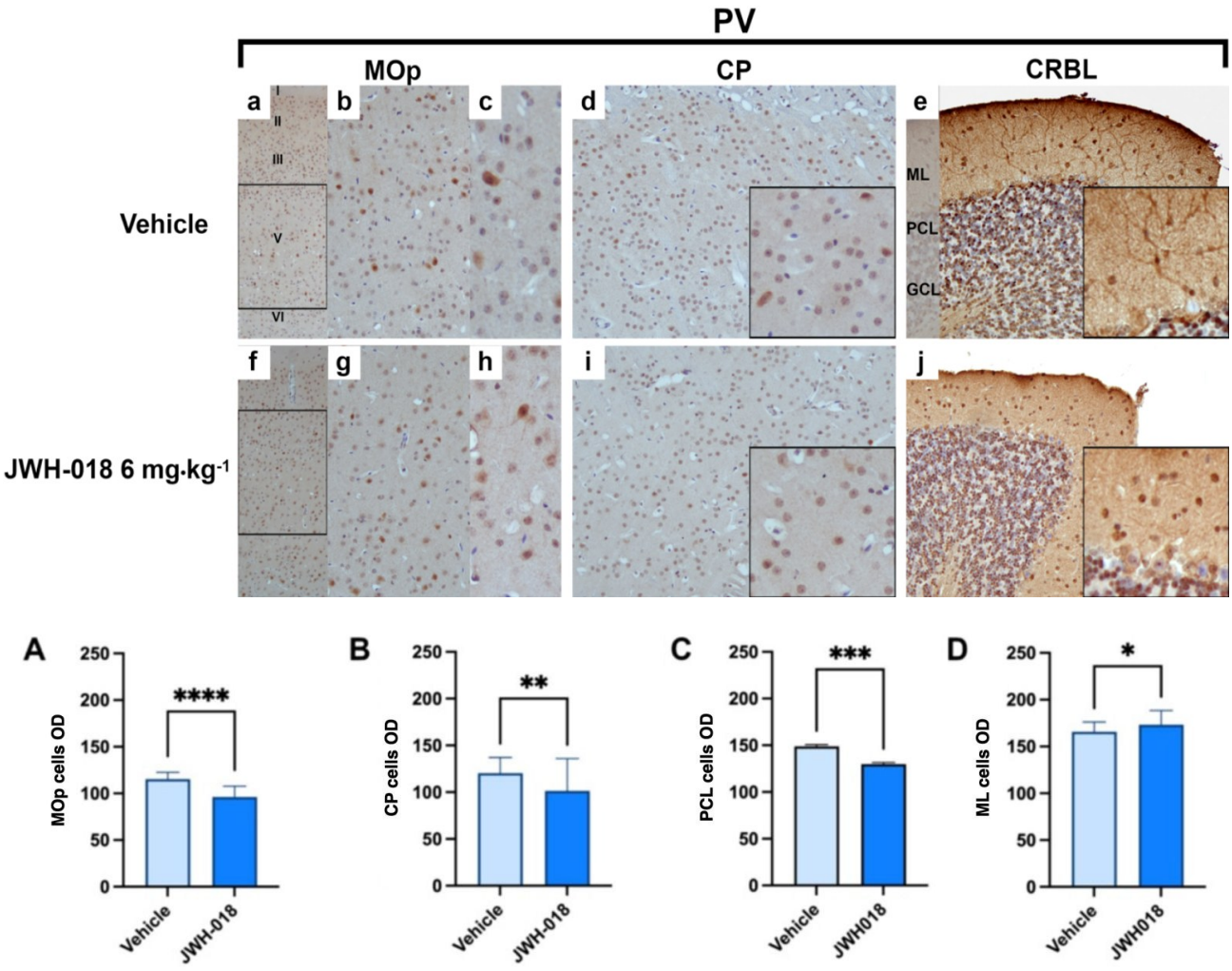


Figure 20. PV immunoreactivity in the MOp, CP, and CRBL in both vehicle- and JWH-018-treated animals. Quantification is presented as OD of immunopositive cells. MOp; a–c and f–h, Panel A: strong PV-immunopositive cell bodies are clearly visible in the control condition across cortical layers (particularly layers V–VI). Following JWH-018 exposure (f–h), there is a visible reduction in DAB staining intensity compared to vehicle (a–c). CP; d and i, Panel B: visible scattered PV-positive interneurons throughout the striatum. The JWH-018 condition (i) exhibits paler, less defined somas compared to the vehicle condition (d). CRBL; e and j, Panels C and D: intense PV labeling is localized to the PCL and the ML, which contains stellate/basket cells and Purkinje dendritic trees.

Calbindin

Highly expressed in the mammalian brain, CALB1 is a major intracellular calcium-binding protein responsible for Ca^{2+} buffering and transport. In the neocortex and striatum, CALB1 is primarily expressed by inhibitory interneurons and caudate medium-sized spiny neurons, respectively, where it regulates calcium homeostasis and overall GABAergic transmission (Pickel & Hares, 1996). In the cerebellar cortex CALB1 represents a highly specific marker for Purkinje cells and works as a crucial determinant of motor coordination (Barski et al., 2003).

Qualitative assessment of CALB1 staining (Fig. 21) of the motor cortex and striatum revealed widespread immunopositivity; specifically, MOp layer V show strong CALB1 signal in both somata and processes, particularly in control specimens. In the cerebellum, vehicle- and JWH-018- treated groups displayed distinct and intense immunopositive Purkinje cells, both in the soma and dendritic arborization, although the latter was much fainter in JWH-018 treated mice. Upon quantification, a statistically significant decrease in CALB1 optical density was detected, within the MOp layer V, in treated animals (41.73 ± 1.38 and 51.96 ± 1.70, for JWH-018 mice and vehicle, respectively) (Fig.21A). Conversely, no significant differences were observed in the caudate-putamen (Fig. 21B). In the cerebellum, particularly within Purkinje cells, a statistically significant reduction in CALB1 immunoreactivity was observed in the treated group compared to vehicle (161.97 ± 2.86 and 170.82 ± 3.21,) (Fig.21C).

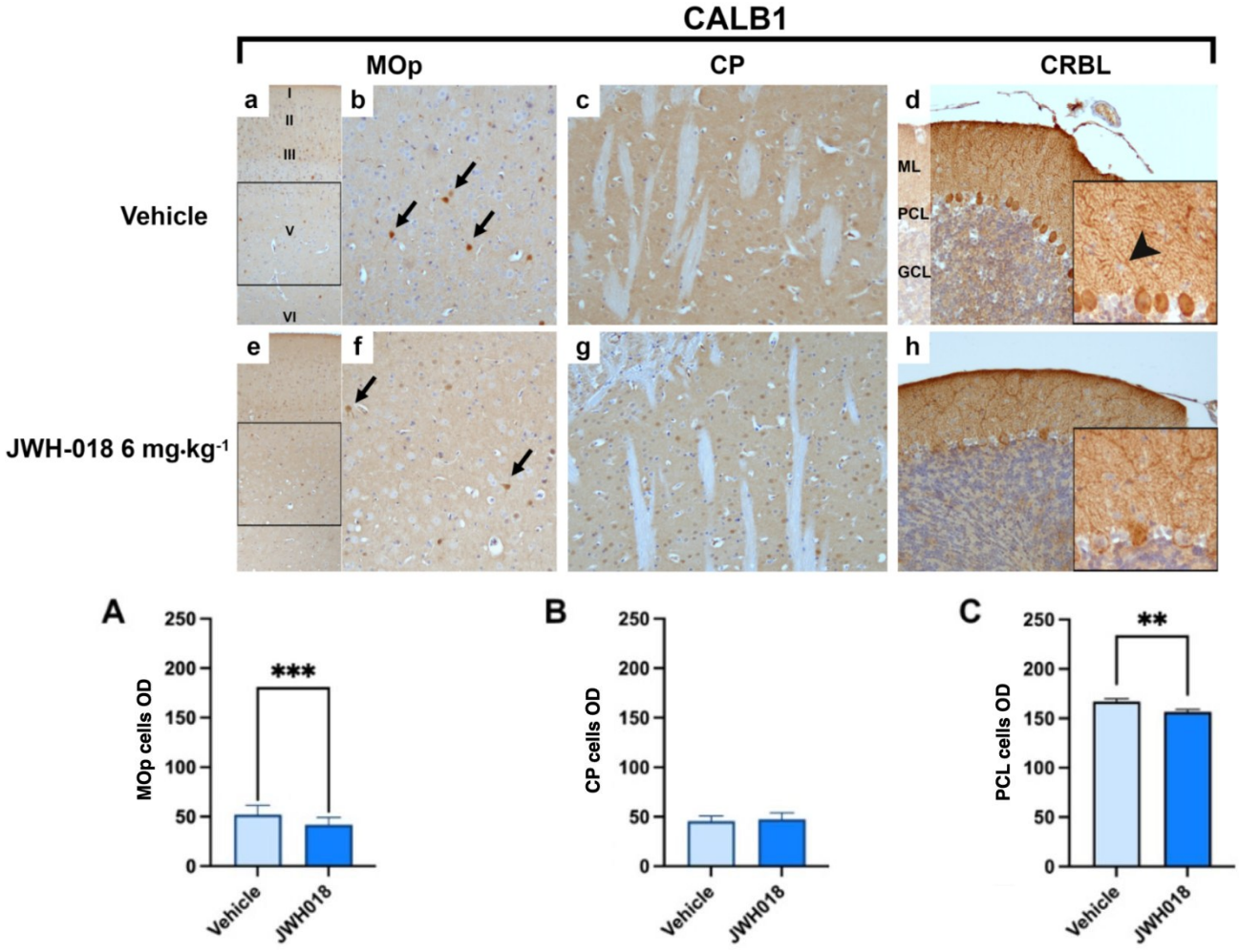


Figure 21. CALB1 immunoreactivity across the MOp, CP, and CRBL and quantitative evaluations of optical density for each brain areas. In the MOp (a, b, e and f), vehicle (a and b) display distinct CALB1-positive interneuron somas and neurites (black arrows in panel b), primarily in intermediate layers, while in JWH-018-treated tissue (e and f), fewer cells are visible (black arrows in panel f) and the staining intensity is noticeably blunted. In the CP (c and g) CALB1 immunopositivity levels are generally lower, and no statistically significant difference (Panel B) is observed between the treated (g) and vehicle (c). In the cerebellar cortex (d and h) CALB1 strongly marks the PCL and their intricate dendritic trees within the ML, particularly evident in vehicle (arrowhead in inset d); in the JWH-018 group (h), the somas in the PCL and the dendritic tree in the ML appear moderately paler and less intensely defined. Panel A-C show histograms for the quantitative evaluation of CALB1 OD analyses in MOp, CP and CRBL, respectively.

Calretinin

Calretinin immunostaining was employed to further characterize calcium homeostasis within specific neuronal populations in specific brain motor areas. Sharing similar features with CALB1, calretinin is a crucial protein with Ca^{2+}-buffering activity widely distributed in the mammalian brain (FN Garas et al., 2018). While CR is highly expressed in the cortex, in the murine striatum CR^{+} interneurons are scarcer (FN Garas et al., 2018); our immunohistochemical analyses (Fig. 22) revealed diffuse CR immunopositivity in the primary motor cortex of both control and treated animals: both cells soma and processes are immunolabeled, although the immunopositivity appeared stronger in the control groups. CR immunopositive signal was very sparse in the caudate-putamen where only very few cells could be detected. In the cerebellar cortex, the immunohistochemical reaction for calretinin revealed the characteristic distribution within the granule cell layer, while CR immune-negative cells were clearly visible in the molecular layer and Purkinje cell layer.

CR immunoreactivity OD analyses in the primary motor cortex revealed a marginally statistically significant reduction in treated animals compared to vehicle (67.850 ± 2.629 and 74.471 ± 3.415, respectively) (Fig.22A), whereas in the caudate putamen of JWH-018-treated mice the decrease in immunopositive cells OD is highly statistically significant compared to the vehicle (101.528 ± 1.476 and 31.327 ± 3.3, for vehicle and JWH-018-treated mice respectively)

(Fig. 22B). Conversely, an opposite trend was observed in the cerebellar granular layer, with a statistically significant immunopositive OD increase in treated animals, compared to vehicles (185.193 ± 3.666 and 151.758 ± 4.310, for JWH-018-treated mice and vehicle respectively) (Fig.22C).

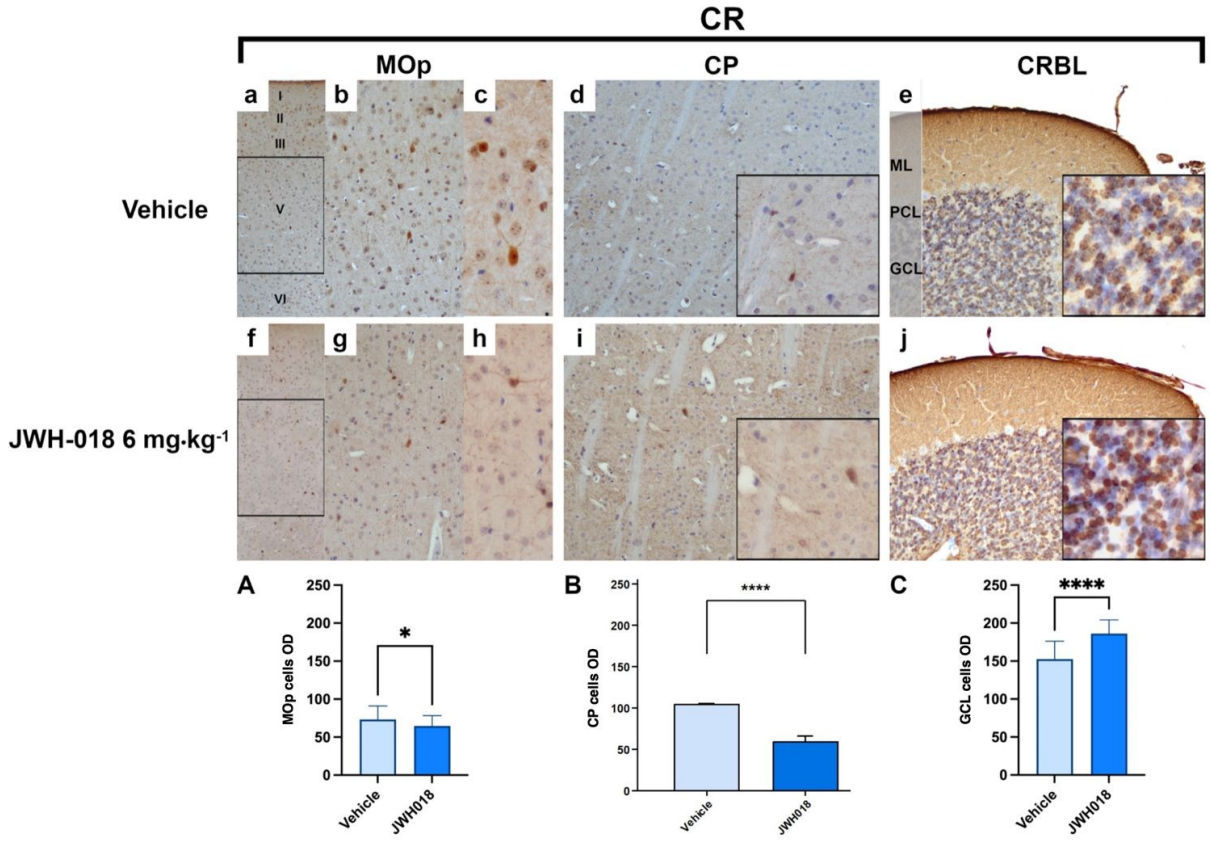


Figure 22. CR immunoreactivity in the MOp, CP, and CRBL. In the MOp (a, b, c, f, g and h) it is possible to observe scattered CR-positive cells across cortical layers in vehicle (a–c); following JWH-018 exposure (f–h), the staining intensity of CR-positive cells are noticeably attenuated compared to vehicle. In the CP (d, i), CR immunoreactivity is highly statistically significant decreased in JWH-treated animals compared to vehicle, as it is also illustrated in the high-magnifications insets (j and i). In the cerebellar cortex (e and j) CR labeling is mainly localized to the GCL and the ML neuropil; within the GCL (high-magnification insets in e and j)), granule cells from JWH-018-treated animals (j) display a distinct increase in cytoplasmic DAB intensity compared to vehicle (e).

6 DISCUSSION

Considering the rapid proliferation of New Psychoactive Substances and their synthetic alternatives to classic drugs, significant regulatory and health challenges have emerged worldwide (A. Shafi et al., 2020). Within this framework, there are synthetic cannabinoid receptor agonists, that target the same cannabinoid receptors as natural phytocannabinoids (May et al., 2019) while escaping conventional THC screenings (Gamage et al., 2019). Based on the established literature, SCRAs behave as full agonists with substantially higher potency and intrinsic efficacy at both CB_1R and CB_2R (I. Vardakou et al., 2010; V. Auwärter et al., 2009; May et al., 2019); in particular, at the level of CNS, main effects are due to CB_1R activation, following which SCRAs strongly modulate dopaminergic transmission and conditioned behaviors, acting in areas such as the prefrontal cortex, ventral tegmental area, nucleus accumbens and ventral pallidum (Canazza et al., 2016; De Luca et al., 2015; Ossato et al., 2016; Di Chiara et al., 2004; Miliano et al., 2016), as well as CB_1- and dopamine-dependent locomotor activity (Ossato et al., 2017; Corli et al., 2025). Beyond forebrain circuits, SCs exert severe neurotoxic damage in motor coordination structures, triggering extensive cell death in the murine cerebellum across multiple signaling pathways, as a recent study on the synthetic cannabinoid AKB-48 has demonstrated (De Luca et al., 2026).

Against this background, considering also the known alteration of the intracellular calcium levels triggered by SCRAs (J.E. Lauckner et al., 2005) and the observed decrease in some of the calcium-binding proteins immunopositivity in CNS cells after the treatment of synthetic cannabinoids (De Luca et al., 2026), this thesis work was focused either on a morphological evaluation and immunohistochemical investigation of the three main calcium-binding protein, to respectively investigate whether JWH-018 treatment may induces morphological alterations within CNS regions such as MOp, CP and CRBL, and to highligth potential alteration in calcium homeostasis as markers of these possible morphological alterations. The histological findings suggest that JWH-018 exposure induces neuroarchitectural damage across distinct motor regions in the mouse brain. Specifically, the marked parenchymal vacuolization observed in both the primary motor cortex and dorsal striatum, alongside hemorrhagic foci in the cerebellum, could be compatible with a pattern of direct neurotoxic injury, as reported in recent literature, where the presence of vacuolization is described in the context of excitotoxicity and may reflect swelling of mitochondria and the endoplasmic reticulum (D. Park et al., 2026). The cerebellar hemorrhagic foci identified after H&E staining are consistent with hemorrhagic change of secondary ischemic injury to cannabinoid-induced cerebrovascular dysfunction, as

supported by experimental data linking synthetic cannabinoids and cannabis to stroke, intracranial hemorrhage, and histopathological evidence of neuronal necrosis, edema, and vascular congestion in the CNS (Filipiuc et al., 2026). This aspect becomes particularly compelling when viewed from a translational standpoint, in which histopathological findings provide critical preclinical evidence supporting clinical observations of synthetic cannabinoid induced cerebrovascular incidents; indeed, in human consumers, acute ischemic stroke and severe cerebrovascular events have been documented even in young, otherwise healthy individuals shortly after SC exposure, phenomena largely attributed to acute cerebral vasospasm, cardio-embolism, and systemic hemodynamic failure with impaired cerebral autoregulation (Moussouttas, 2004). Another study performing post-mortem morphological assessments on the brain of a young woman following a fatal MDMB-4en-PINACA and 4F-ABUTINACA overdose documented both macroscopic and histological cerebral edema (G. Simon et al., 2023). In this framework, it is plausible to hypothesize a link between the observed neuropil vacuolization and a possible early phase of ischemic brain edema, which is predominantly cytotoxic in nature; cytotoxic edema could arise from increased cell membrane permeability, impaired energy-dependent active transport, or a combination of both mechanisms (A. Baethmann, 1978). In this regard, the link between synthetic cannabinoid intake and mitochondrial dysfunction becomes particularly interesting; investigations into SCs-induced neurotoxicity have documented a collapse in mitochondrial membrane potential within neuroblastoma models (I. Canazza et al., 2017). Furthermore, mitochondrial dysfunction and defective motility have emerged as primary toxicological drivers; specifically, intramitochondrial $G_{\alpha i}$ protein coupling suppresses soluble adenylyl cyclase activity, attenuating PKA-dependent phosphorylation of electron transport chain components and ultimately arresting cellular respiration (Hebert-Chatelain E et al., 2016; Alexandre J et al., 2020). This metabolic impairment is accompanied by oxidative and inflammatory cascades: the SC APINACA exposure in SH-SY5Y neuroblastoma cells promotes ROS accumulation and upregulates CB1R, MAPK8, IL-6, and TNF-alpha, a pro-oxidant effect similarly elicited by JWH-018 (Oztas E et al., 2019; Sezer et al., 2020). In literature is known that the pharmacological profile of SCs could extend beyond classical CB1R/CB2R to encompass non-cannabinoid central targets, including GPR55, GPR18, PPARs, and TRPV1 channels (A. Alz'ubi et al., 2024); in this context GPR55 engagement stimulates $G_{12/13\text{-}Rho}$ signaling, raising intracellular Ca^{2+} to drive BBB breakdown, oxidative stress, and neuroinflammation (Morales P and Jagerovic N et al., 2016; Lauckner JE et al., 2008; Leo LM et al., 2019). Similarly, GPR18 fosters microglial neuroinflammatory responses via CB2R interactions (Reyes-Resina I et al., 2018). Ultimately, although SC-mediated activation of nuclear PPAR isoforms typically yields neuroprotective

and antioxidant effects (O'Sullivan S., 2019), intense CB1R overactivation by SCs can uncouple this protection to fuel oxidative distress (Iannotti FA and Vitale RM., 2021). Moreover, it was demonstrated that SCs like XLR-11 can directly open TRPV1 channels, accelerating neuronal Ca^{2+} overload (Andersen H and Walsh K., 2021).

In parallel, immunohistochemical evaluation of main CaBPs, through a quantification of immunopositivity based on OD levels, highlighted an area-specific immunopositive trend, as well as distinct patterns that are specific to both calcium-binding protein labeling and layers within the same areas. Calcium-binding proteins, specifically parvalbumin, calbindin, and calretinin, have been extensively investigated over the past decades owing to their distinctive, cell-type-specific distribution across the CNS. These markers delineate specialized neuronal subpopulations, often serving as reliable neurochemical signatures; parvalbumin is predominantly expressed by inhibitory GABAergic interneurons, including cortical and hippocampal basket cells (Contreras D., 2004), distinct retinal amacrine subsets (Lee ES and Jeon CJ, 2013), cerebellar Purkinje cells (Chen G. at al., 2006) and diverse cortical interneurons (Clements R.J. et al., 2008); however, it is also present in excitatory glutamatergic populations, such as specific retinal ganglion cells (Yi C.W. et al., 2012) and corticostriatal projection neurons (Jinno S., and Kosaka T., 2004). Calbindin displays a broad localization profile that encompasses cerebellar Purkinje neurons (Celio M.R., 1990; Kim B.J. et al., 2009), hippocampal dentate granule and superficial CA1 pyramidal cells, and cortical circuits (Van Brederode J.F. et al., 1991). Calretinin, initially discovered in the retina where it labels ganglion, amacrine, and horizontal cells, is also prominent in cortical and hippocampal interneurons, alongside cerebellar granule cells (Barinka F. and Druga R., 2009; Resibois A. and Rogers J.H., 1992). Collectively, CaBPs display distinct functional properties tailored to the intrinsic excitability and synaptic dynamics of the neuronal populations harboring them; nevertheless, substantial variations in their calcium-buffering capacities, binding kinetics, and intracellular expression levels may crucially dictate differential neuronal vulnerability against pathological, toxic elevations of intracellular calcium (R. Fairless et al., 2019). Such an evaluation of immunopositivity levels makes sense, given that synthetic cannabinoids have already been observed to cause an alteration in intracellular calcium homeostasis (J.E. Lauckner et al., 2005). An uncontrolled accumulation of Ca^{2+} within the neuronal cytosol and nucleus could represent the final common pathway leading to hypoxic-ischemic cell death and neurodegeneration (Mishra OP, Delivoria-Papadopoulos M, 1999). Sustained elevations in intracellular calcium levels are typically triggered by diverse metabolic stresses, such as oxidative stress (Christakos et al, 2000), and occur through several

concurrent mechanisms. These include the influx of extracellular calcium via voltage- and ligand-gated channels, as well as its release from internal stores such as the endoplasmic reticulum and mitochondria (Siesjo BK et al., 1999; Zanelli SA et al., 1999). This cytosolic overload is frequently exacerbated by the failure of physiological clearance systems, including the impairment of endogenous buffering capacity, organelle sequestration, and active extrusion pumps.

The selective reduction of PV immunoreactivity observed in the primary motor cortex and caudate putamen in JWH-018-treated mice is particularly intriguing when interpreted against existing neuropathological models of cortical vulnerability. In pathological conditions characterized by neuroinflammatory or excitotoxic stress, such as Multiple Sclerosis, a selective downregulation or loss of PV-containing GABAergic interneurons has been directly linked to perturbations in intracellular Ca^{2+} homeostasis (Dutta et al., 2006); given that synthetic cannabinoids can trigger non-canonical G_q/PLC-mediated release of Ca^{2+} from intracellular endoplasmic reticulum stores (Lauckner et al., 2005) while driving persistent CB_1R overactivation, PV-expressing interneurons in the primary motor cortex may be unable to buffer this acute calcium surge, leading to their selective functional downregulation or structural loss. An alternative interpretation could arise from genetic evidence demonstrating that genetic ablation of the CB_1 receptor ($CB_1^{-/-}$ mice) leads to a marked downregulation of PV immunolabeling in the primary motor cortex, alongside similar reductions in the prefrontal cortex and striatum (Fitzgerald et al., 2012). In this scenario, the decrease in PV expression observed in our treated animals could reflect a secondary effect driven by a functional loss or profound downregulation of CB_1 receptors on interneurons. Because JWH-018 acts as a high-efficacy, high-affinity full agonist, sustained exposure may trigger massive receptor internalization, desensitization, or exhaustion of downstream signaling, thereby explaining the localized reduction in PV levels as a compensatory adaptation to chronic cannabinoid overstimulation (Sim-Selley Laura J., 2003). It's important to consider that within the caudate-putamen, fast-spiking PV^+ interneurons exert a dominant, feed-forward inhibitory control over striatal projection neurons (Koós and Tepper, 1999; Tepper et al., 2004). Clinical and preclinical models of basal ganglia disorders demonstrate that the selective depletion or hypofunction of striatal PV^+ interneurons impairs this feed-forward inhibition, culminating in aberrant projection neuron activity and the emergence of severe motor disturbances, including dystonia and motor uncoordination (Reiner et al., 2013). In line with this pathophysiology framework other experimental findings strongly align with such basal ganglia dysregulation: the administration of

JWH-018–6-OMe produced a pronounced suppression of spontaneous locomotor activity in parallel with robust cataleptic immobility (S. Khan et al., 2026).

In parallel with the alterations observed in parvalbumin-containing interneurons, the investigation of CALB1 provided further insight into the disruption of cortical and striatal calcium dynamics. Classically, CALB1 in MOp delineates two main neuronal pools: interneurons in layers II–III and V, and moderately stained pyramidal neurons in upper layers, framed by prominent bundles of immunoreactive processes (Xue-Zhi Sun et al., 2002); in the rodent caudate-putamen, calbindin is expressed in medium spiny projection neurons and selectively delineates the striatal matrix compartment, while the striosome/patch compartment remains essentially devoid of CALB1 immunoreactivity (Gerfen et al., 1985). The immunohistochemical evaluation of CALB1 immunoreactivity showed a statistically significant decreasing trend in the MOp; together with PV decrease, the reduction of calbindin levels, further supports loss of calcium homeostasis upon JWH-018 administration. Indeed, in paradigms of normal aging and neurodegenerative disorders, significant declines in calbindin gene expression have been directly implicated in depleting the neuron's capacity to buffer cytosolic free calcium, thereby rendering vulnerable cells susceptible to calcium-mediated, irreversible cytotoxic cascades (M.Iacopino and S. Christakos, 1990). A particularly revealing parallel emerges when comparing our findings with the neuropathological alterations documented in basal ganglia and cortical movement disorders: in clinical and post-mortem studies of Huntington's disease (HD) presenting with severe motor symptoms, calbindin-positive (CB+) interneurons within laminae II/III and V of the primary motor cortex display a profound and selective morphological degeneration, characterized by marked somal shrinkage and extensive dendritic pruning, that spares other interneuronal subclasses (Kim et al., 2014). Importantly, the decrease in calbindin-positive cells OD observed in our study would mirror neuropathological patterns triggered by other major substances of abuse: in rodent models of methamphetamine neurotoxicity, exposure induces substantial and persistent damage to cortical interneurons, resulting in loss of CB^{+} interneurons in middle-to-deep neocortical layers (Kuczenski et al., 2007).

To complete the immunohistochemical assessment concerning calcium-binding proteins in the MOp and caudate-putamen, the study examined the levels of calretinin immunopositivity. Within the neocortex, CR-positive interneurons represent a heterogeneous subpopulation accounting for approximately 10–30% of all GABAergic interneurons, and are concentrated predominantly in superficial layers (II–III), with a density that decreases in infragranular layers (Barinka and Druga, 2010; B. Cauli et al., 2014). The results of this study showed a diminishing level of calretinin-immunopositive cells in the MOp and CP in JWH-treated mice compared to vehicle; this is likely a pathological effect driven

by the high potency of the synthetic treatment, which may disrupt physiological calcium homeostasis and impose a sustained calcium-buffering burden on neurons. In this context, the observed reduction in CR may reflect a maladaptive loss of calcium-buffering capacity, as decreased levels of calcium-binding proteins, including calretinin, have been reported in pathological conditions associated with calcium dysregulation (Zong et al., 2025).

In contrast to the motor cortex and striatum, immunohistochemical examination of the cerebellum, following JWH-018 administration, revealed an opposing, in layer-specific profile for parvalbumin. Specifically, a marked reduction in PV immunoreactivity was detected across the PCs layer, whereas the molecular layer exhibited a concomitant increase. The cerebellum represents one of the brain regions with the highest density of cannabinoid type-1 receptors, making it an exceptionally sensitive target for cannabinoid (Kawamura et al. 2006). Classical behavioral and neuropharmacological studies have well established that *in vivo* administration of synthetic CB_1 receptor agonists in rodents severely disrupts cerebellum-dependent motor coordination, postural balance, and fine motor control (DeSanty and Dar, 2001; Patel and Rillard, 2001). The decrease in PV-immunoreactivity of PCs to JWH-018 closely mirrors recent neurotoxicological evidence reported in a study demonstrating that synthetic cannabinoids can induce cell death within the murine cerebellum across multiple distinct signaling cascades (De Luca et al., 2026); furthermore, electrophysiological investigations have demonstrated that potent synthetic cannabinoid receptor agonists, such as MAM-2201, strongly suppress excitatory synaptic transmission onto PCs via the robust activation of presynaptic CB_1 receptors located on parallel fiber and climbing fiber terminals (Tomohiko et al., 2015). By decreasing presynaptic glutamate release probability, synthetic CB_1R agonists significantly attenuate excitatory postsynaptic currents and depress spontaneous PC firing, which would explain a decrease in the level of PV immunopositivity. However, the significant upregulation of parvalbumin-positive cells in the molecular layer introduces a contrasting note, although it could be consistent with literature reporting distinct patterns of intensity and subcellular distribution. Purkinje cells show diffuse granular cytoplasmic parvalbumin immunoreactivity in the soma and dendrites, with weaker nuclear staining, and frequently co-express calbindin, whereas molecular layer interneurons exhibit very strong parvalbumin labeling in the soma, axons and synaptic terminals, often exceeding the intensity observed in Purkinje cell bodies, which may indicate a shift in the relative contribution of PV-positive cellular compartments, with reduced Purkinje-cell somatic labeling accompanied by a proportionally greater signal from molecular layer interneurons and/or their axonal and synaptic plexus (Caillard et al., 2000).

A decreasing trend was also noticed in calbindin-immunopositive cells OD concerning the PCs layer, a trend consistent with results of other studies evaluating the effects of the synthetic cannabinoid AKB-48, where this pattern supports the activation of specific apoptotic or neurotoxic cascades in these cells (De Luca et al., 2026). Classically, the progressive downregulation of calbindin in Purkinje cells during paraneoplastic cerebellar degeneration exemplifies the vital function of this protein in sustaining neuronal Ca^{2+} homeostasis (De Luca et al., 2026). This loss of calbindin takes on particular significance when considering the distinctive physiology of cerebellar Purkinje cells. PCs are notoriously characterized by a selective vulnerability to both natural and experimental hypoxic/ischemic insults, at times displaying an even higher susceptibility than other fragile neuronal populations, such as hippocampal pyramidal cells (Sato M et al., 1990; Cervos-Navarro J and Diemer NH, 1991). However, the precise reasons underlying this heightened sensitivity is not completely understood, even if it has been largely linked to their high expression of AMPA receptors that exhibit slow or incomplete desensitization, ultimately favoring the deleterious build-up of toxic intracellular calcium transients (Brorson JR *et* al., 1995; Tomiyama M et al., 1999). At physiological state, PCs operate under substantial metabolic and ionic demands: they maintain high spontaneous firing rates and generate multiphasic "complex spikes" that trigger massive, rapid redistributions of Ca^{2+} from intracellular stores and across dendrites (Braitenberg et al., 1997; Volpe et al., 1997); to manage these heavy ionic loads, PCs rely on an elaborate machinery consisting of rapid sequestration by intracellular organelles, plasma membrane Ca^{2+}-ATPase extrusion, and high concentrations of endogenous calcium-binding proteins (Talamoni et al., 1997). Among these buffers, calbindin is fundamental for its pivotal physiological contribution to calcium homeostasis and the modulation of neuronal excitability (Airaksinen MS et al., 1997); indeed, abundant evidence points to a neuroprotective and excitoprotective role for calbindin against calcium-mediated cytotoxic damage (Christakos et al, 2000), while its downregulation has been repeatedly documented across various models of oxidative stress, such as rodent aging (Iacopino et al., 1990), or morphine exposure (Garcia et al., 1996). Although the exact degree to which calbindin elevation confers excitoprotection remains subject to debate,the selective reduction in calbindin immunoreactivity observed in our results could suggest that JWH-018 administration may compromise the primary calcium-buffering system of PCs.

Lastly, the study examined the immunoreactivity of CR^{+} cells in the cerebellum; in the cerebellar cortex, calretinin is prominently expressed in the granular layer, where it labels granule cells and their parallel fibers (Rogers, 1987). The results of this thesis revealed an increase in the CR^{+} immunoreactivity OD, thus showing a contrasting behaviour compared to the previous two calcium-binding

proteins, i.e. parvalbumin and calbindin. This divergent profile is particularly revealing when framed within the intrinsic electrophysiological architecture of the input stage of the cerebellar cortex. Cerebellar granule cells exhibit a strict, calcium-dependent tuning of their intrinsic excitability and firing dynamics (D'Angelo et al., 1997). A work by Gall and colleagues (2003) demonstrated that endogenous calretinin acts as the critical cytosolic buffer governing granule cell electroresponsiveness; indeed, the absence or depletion of calretinin precipitates severe alterations in action potential generation and signal coding, a deficit that can be fully rescued by restoring cytosolic buffering capacity (Gall et al., 2003). The opposite changes in calretinin versus calbindin/parvalbumin immunoreactivity are consistent with their localization in distinct cerebellar cellular compartments. Thus, these findings may reflect differential regulation of calcium-buffering proteins in anatomically and functionally distinct components of the cerebellar cortical circuit in response to the modulation of cerebellar circuits induced by JWH-018 (Fortin et al., 1998; Empson and Knöpfel, 2010).

A compelling finding emerging from our immunohistochemical analysis is the divergence in calcium-binding protein dynamics between forebrain motor structures and the cerebellum following the synthetic cannabinoid JWH-018 administration. While both the caudate-putamen and MOp exhibit an unambiguous, concurrent downregulation across all three markers (i.e parvalbumin, calbindin, and calretinin), the cerebellar cortex displays layer-specific heterogeneity, marked by the preservation or selective upregulation of specific calcium buffers, such as calretinin in the granule cell layer and parvalbumin in the molecular stratum. This discrepancy could find an explanation in the differential kinetics of CB_1 receptor regulation and transcriptional adaptation described across distinct brain areas during sustained cannabinoid exposure. As demonstrated by Zhuang and colleagues, chronic cannabinoid administration elicits marked, region-specific divergence in CB_1 receptor mRNA expression and functional desensitization across the striatum, hippocampus, and cerebellum (Zhuang et al., 1998); specifically, CB_1 mRNA levels in the caudate-putamen show only relative decreases and never exceed vehicle control values even after protracted exposure (Rubino et al., 1994). In an environment where sustained agonist stimulation maintains prolonged downstream effector perturbation, such as persistent suppression of cAMP (Dill and Howlett, 1988; Howlett, 1985) and altered conductances of calcium and potassium channels (Deadwyler et al., 1995; Mackie, Hille, 1992), striatal microcircuits are supposed to be vulnerable to protracted calcium dysregulation. In contrast, the cerebellar cannabinoid system engages distinct adaptive dynamics under chronic agonist challenge (Zhuang et al., 1998). Within the cerebellar cortex, CB_1 receptor expression exhibits clear biphasic alterations characterized by early desensitization followed by a transient, robust increase in CB_1 mRNA synthesis (Fan et al.,

1996). This rapid compensatory induction of receptor mRNA reflects an intrinsic capacity of cerebellar microcircuits to restore effector balance in response to severe receptor-G protein uncoupling (Breivogel et al., 1998). In light of the aforementioned literature, the divergent patterns observed between the striatum and cerebellum can be interpreted as a consequence of the cerebellum's ability to rapidly mitigate excessive cannabinoid signaling through accelerated desensitization and subsequent transcriptional recalibration, thanks to which local neurons are not subjected to the same continuous, unbuffered excitotoxic burden seen in the striatum. Consequently, distinct cerebellar compartments retain the capacity to deploy active homeostatic responses.

7 CONCLUSIONS

The findings of this thesis work address an urgent, real-world public health issue. Synthetic cannabinoids continue to spread rapidly on the illicit market, often falsely advertised as safe, legal alternatives to natural cannabis while remaining undetected by standard drug tests. In recent years, fueled by growing social distress following the pandemic, substance abuse has increased significantly, speeding up the shift from casual, weekend use to dangerous addiction (Simão et al., 2022). In this context, understanding how these substances truly affect the brain is critical. The data reported in the present study suggest that synthetic cannabinoids may drive loss of calcium homeostasis in crucial motor areas, whose underlying mechanisms deserve further investigation to better understand how this may lead to CNS dysfunctions. However, this study has some limitations, such as: direct real-time quantification of intracellular calcium levels was not performed, an aspect that future studies should address via dedicated calcium imaging or fluorometric assays. Furthermore, a possible dysregulation of the glutamatergic pathway was not directly evaluated to corroborate the possible excitotoxic mechanism activation. Future research should therefore integrate targeted molecular approaches, specifically RT-qPCR and Western blotting, alongside functional calcium assessments to fully elucidate the downstream pathways and molecular targets involved.

The practical value of this study lies in bridging laboratory research with clinical care. A clearer characterization of the central pathways involved in synthetic cannabinoid–induced neurotoxicity may aid emergency clinicians in recognizing atypical toxidromes, thereby optimizing risk stratification and the supportive management of acutely intoxicated patients. Furthermore, uncovering these injury mechanisms is a key step toward developing treatments that can protect brain cells during drug exposure, while offering public health authorities solid evidence to warn the community and better regulate these hazardous compounds.

8 BIBLIOGRAPHY

Adkins-Regan E. Comparative Vertebrate Neuroanatomy: Evolution and Adaptation. Trends Neurosci. 1997;20:229.

Ahn KH, et al. Distinct roles of β-arrestin 1 and β-arrestin 2 in ORG27569-induced biased signaling and internalization of the cannabinoid receptor 1 (CB1). J Biol Chem. 2013;288:9790-9800.

Airaksinen MS et al. Ataxia and altered dendritic calcium signaling in mice carrying a targeted null mutation of the calbindin D28k gene. Proc Natl Acad Sci U S A. 1997; 94:1488-1493.

Alexandre J et al. The Synthetic Cannabinoids THJ-2201 and 5F-PB-22 Enhance In Vitro CB1 Receptor-Mediated Neuronal Differentiation at Biologically Relevant Concentrations. Int J Mol Sci. 2020; 21:8422.

Alger BE. Retrograde signaling in the regulation of synaptic transmission: focus on endocannabinoids. Prog Neurobiol. 2002;68:247-286.

Allen NJ, Eroglu C. Cell biology of astrocyte-synapse interactions. Neuron. 2017;96:697-708.

Andersen HK, Walsh KB. Molecular signaling of synthetic cannabinoids: Comparison of CB1 receptor and TRPV1 channel activation. Eur J Pharmacol. 2021; 907:174301.

Andersson M, et al. Metabolic profiling of new synthetic cannabinoids AMB and 5F-AMB by human hepatocyte and liver microsome incubations and high-resolution mass spectrometry. Rapid Commun Mass Spectrom. 2016;30:1067-1078.

Ango F, et al. Bergmann glia and the recognition molecule CHL1 organize GABAergic axons and direct innervation of Purkinje cell dendrites. PLoS Biol. 2008;6:e103.

Aponte Y, Bischofberger J, Jonas P. Efficient Ca2+ buffering in fast-spiking basket cells of rat hippocampus. J Physiol. 2008;586:2061-2075.

Apps R, et al. Cerebellar modules and their role as operational cerebellar processing units. Cerebellum. 2018;17:654-682.

Apps R, Hawkes R. Cerebellar cortical organization: a one-map hypothesis. Nat Rev Neurosci. 2009;10:670-681.

Argyropoulos GP, et al. The cerebellar cognitive affective/Schmahmann syndrome: a task force paper. Cerebellum. 2020;19:102-125.

Ashton JC, et al. Expression of the cannabinoid CB2 receptor in the rat cerebellum: an immunohistochemical study. Neurosci Lett. 2006;396:113-116.

Atwood BK et al. JWH018, a common constituent of 'Spice' herbal blends, is a potent and efficacious cannabinoid CB1 receptor agonist. Br J Pharmacol. 2010; 160(3):585-593.

Auwärter V, et al. 'Spice' and other herbal blends: harmless incense or cannabinoid designer drugs? J Mass Spectrom. 2009;44:832-837.

Baethmann, A. Pathophysiological and pathochemical aspects of cerebral edema. Neurosurgical Review, 1978, 1.3: 85-100.

Barbieri M, et al. Synthetic cannabinoid JWH-018 and its halogenated derivatives JWH-018-Cl and JWH-018-Br impair Novel Object Recognition in mice: Behavioral, electrophysiological and neurochemical evidence. Neuropharmacology. 2016;109:254-269.

Barinka F, Druga R. Calretinin expression in the mammalian neocortex: a review. Physiol Res. 2010;59:665-677.

Barmack NH, Yakhnitsa V. Functions of interneurons in mouse cerebellum. J Neurosci. 2008;28:1140-1152.

Barski JJ, et al. Calbindin in cerebellar Purkinje cells is a critical determinant of the precision of motor coordination. J Neurosci. 2003;23:3469-3477.

Barthas F, Kwan AC. Secondary Motor Cortex: Where 'Sensory' Meets 'Motor' in the Rodent Frontal Cortex. Trends Neurosci. 2017;40:181-193.

Bilel S, et al. Cognitive dysfunction and impaired neuroplasticity following repeated exposure to the synthetic cannabinoid JWH-018 in male mice. Br J Pharmacol. 2023;180:2777-2801.

Braitenberg V et al. The detection and generation of sequences as a key to cerebellar function. Experiments and theory. Behav Brain Sci. 1997; 20:229-277.

Britzolaki A et al. The SERCA2: a gatekeeper of neuronal calcium homeostasis in the brain. Cell Mol Neurobiol. 2018; 38(5):981-994.

Brorson JR et al. AMPA receptor desensitization predicts the selective vulnerability of cerebellar purkinje cells to excitotoxicity. J Neurosci. 1995; 15:4515-4524

Brown SP, Safo PK, Regehr WG. Endocannabinoids inhibit transmission at granule cell to Purkinje cell synapses by modulating three types of presynaptic calcium channels. J Neurosci. 2004;24:5623-5631.

Bucher EA, et al. Coherence and cognition in the cortex: the fundamental role of parvalbumin, myelin, and the perineuronal net. Brain Struct Funct. 2021;226:2041-2055.

Caillard O, et al. Role of the calcium-binding protein parvalbumin in short-term synaptic plasticity. Proc Natl Acad Sci U S A. 2000;97:13372-13377.

Canazza I et al. Pharmaco-toxicological effects of the novel third-generation fluorinate synthetic cannabinoids, 5F-ADBINACA, AB-FUBINACA, and STS-135 in mice. In vitro and in vivo studies. Hum Psychopharmacol. 2017; 32:e2601.

Canazza I, et al. Effect of the novel synthetic cannabinoids AKB48 and 5F-AKB48 on "tetrad", sensorimotor, neurological and neurochemical responses in mice. In vitro and in vivo pharmacological studies. Psychopharmacology (Berl). 2016;233:3685-3709.

Carafoli E, Crompton M. The regulation of intracellular calcium. Curr Top Membr Transp. 1978;10:151-216.

Cardiff RD, Miller CH, Munn RJ. Manual hematoxylin and eosin staining of mouse tissue sections. Cold Spring Harb Protoc. 2014;2014:pdb.prot073411.

Carlier J, Diao X, Huestis MA. Synthetic cannabinoid BB-22 (QUCHIC): Human hepatocytes metabolism with liquid chromatography-high resolution mass spectrometry detection. J Pharm Biomed Anal. 2018;157:27-35.

Cauli B, et al. Revisiting enigmatic cortical calretinin-expressing interneurons. Front Neuroanat. 2014;8:52.

Celio M.R. Calbindin D-28k and parvalbumin in the rat nervous system. Neuroscience. 1990; 35:375–475.

Cervos-Navarro J, Diemer NH. Selective vulnerability in brain hypoxia. Crit Rev Neurobiol. 1991; 6:149-182.

Cesana E, et al. Granule cell ascending axon excitatory synapses onto Golgi cells implement a potent feedback circuit in the cerebellar granular layer. J Neurosci. 2013;33:12430-12446.

Cha HJ, et al. Neurotoxicity of synthetic cannabinoids JWH-081 and JWH-210. Biomol Ther (Seoul). 2015;23:597-603.

Chen G et al. Deficiency in parvalbumin, but not in calbindin D-28k upregulates mitochondrial volume and decreases smooth endoplasmic reticulum surface selectively in a peripheral, subplasmalemmal region in the soma of Purkinje cells. Neuroscience. 2006; 142:97–105.

Cheng FY, Fleming JT, Chiang C. Bergmann glial Sonic hedgehog signaling activity is required for proper cerebellar cortical expansion and architecture. Dev Biol. 2018;440:152-166.

Christakos et al. Activation of programmed cell death by calcium: protection against cell death by the calcium binding protein, calbindin-D28k. In: Calcium: The molecular basis of calcium action in biology and medicine. Dordrecht: Springer Netherlands, 2000. p. 259-275.

Clapham DE. Calcium signaling. Cell. 2007;131:1047-1058.

Clements RJ et al. Distribution of parvalbumin and calretinin immunoreactive interneurons in motor cortex from multiple sclerosis post-mortem tissue. Exp Brain Res. 2008; 187:459–465.

Colonna M, Butovsky O. Microglia function in the central nervous system during health and neurodegeneration. Annu Rev Immunol. 2017;35:441-468.

Connor JA, et al. Calcium signals in long-term potentiation and long-term depression. Can J Physiol Pharmacol. 1999;77:722-734.

Contreras D. Electrophysiological classes of neocortical neurons. Neural Netw. 2004;17:633–646

Corli G, et al. Repeated treatment with JWH-018 progressively increases motor activity and aggressiveness in male mice: involvement of CB1 cannabinoid and D1/D2 dopaminergic receptors. Eur J Pharmacol. 2025;998:177633.

Cravatt BF et al. Molecular characterization of an enzyme that degrades neuromodulatory fatty-acid amides. Nature. 1996; 384(6604):83-87.

D'Angelo E et al. The cerebellar Golgi cell and spatiotemporal organization of granular layer activity. Front Neural Circuits. 2013; 7:93.

D'Angelo E, et al. Synaptic activation of Ca2+ action potentials in immature rat cerebellar granule cells in situ. J Neurophysiol. 1997;78:1631-1642.

De Luca F, et al. The Synthetic Cannabinoid AKB-48 Induces Cell Death in Murine Cerebellum Through Different Signaling Pathways. Int J Mol Sci. 2026;27:3867.

De Luca MA, et al. Stimulation of in vivo dopamine transmission and intravenous self-administration in rats and mice by JWH-018, a Spice cannabinoid. Neuropharmacology. 2015;99:705-714.

Deadwyler SA. Functional significance of cannabinoid receptors in brain. In: Pertwee RG, editor. Cannabinoid receptors. Academic Press; 1995. p. 205-231.

DeFelipe J, et al. New insights into the classification and nomenclature of cortical GABAergic interneurons. Nat Rev Neurosci. 2013;14:202-216.

DeSanty KP, Dar MS. Cannabinoid-induced motor incoordination through the cerebellar CB1 receptor in mice. Pharmacol Biochem Behav. 2001;69:251-259.

Di Chiara G, et al. Dopamine and drug addiction: the nucleus accumbens shell connection. Neuropharmacology. 2004;47 Suppl 1:227-241.

Dill JA, Howlett AC. Regulation of adenylate cyclase by chronic exposure to cannabimimetic drugs. J Pharmacol Exp Ther. 1988;244:1157-1163.

Dolphin AC. Functions of presynaptic voltage-gated calcium channels. Function (Oxf). 2021; 2(1):zqaa027.

Duchen MR. Mitochondria and Ca2+ in cell physiology and pathophysiology. Cell Calcium. 2000; 28(5-6):339-348.

Dutta R, et al. Mitochondrial dysfunction as a cause of axonal degeneration in multiple sclerosis patients. Ann Neurol. 2006;59:478-489.

Empson RM, Knöpfel T. Functional integration of calcium regulatory mechanisms at Purkinje neuron synapses. Cerebellum. 2012;11:640-650.

Fahrion JK, et al. Cerebellar patterning. In: Rubenstein J, Rakic P, editors. Comprehensive Developmental Neuroscience: Patterning and Cell Type Specification in the Developing CNS and PNS. Elsevier; 2013. p. 199-221.

Fairless R, Williams SK, Diem R. Calcium-binding proteins as determinants of central nervous system neuronal vulnerability to disease. Int J Mol Sci. 2019;20:2146.

Fan F, et al. Cannabinoid receptor down-regulation without alteration of the inhibitory effect of CP 55,940 on adenylyl cyclase in the cerebellum of CP 55,940-tolerant mice. Brain Res. 1996;706:13-20.

Faust TW, et al. Neostriatal GABAergic interneurons mediate cholinergic inhibition of spiny projection neurons. J Neurosci. 2016;36:9505-9511.

Filipiuc SI, et al. Acute toxicity of three synthetic cannabinoids: first in vivo preclinical study. Molecules. 2026;31:2365.

Fischer AH, et al. Hematoxylin and eosin staining of tissue and cell sections. Cold Spring Harb Protoc. 2008;2008:pdb.prot4986.

Fisyunov A, et al. Cannabinoids modulate the P-type high-voltage-activated calcium currents in Purkinje neurons. J Neurophysiol. 2006;96:1267-1277.

FitzGerald MJ, Gruener G, Mtui E. FitzGerald's Clinical Neuroanatomy and Neuroscience. 7th ed. Elsevier; 2015.

Fitzgerald ML, Shobin E, Pickel VM. Cannabinoid modulation of the dopaminergic circuitry: implications for limbic and striatal output. Prog Neuropsychopharmacol Biol Psychiatry. 2012;38:21-29.

Fortin M, Marchand R, Parent A. Calcium-binding proteins in primate cerebellum. Neurosci Res. 1998;30:155-168.

Franklin KBJ, Paxinos G. Paxinos and Franklin's the Mouse brain in stereotaxic coordinates, compact: The coronal plates and diagrams. 5th ed. London: Elsevier, 2019.

Fu Y et al. Precerebellar cell groups in the hindbrain of the mouse defined by retrograde tracing and correlated with cumulative Wnt1-Cre genetic labeling. Cerebellum. 2011; 10(3):570-584.

Fu Y, et al. Precerebellar cell groups in the hindbrain of the mouse defined by retrograde tracing and correlated with cumulative Wnt1-cre genetic labeling. Cerebellum. 2011;10:570-584.

Gabbott PL, Bacon SJ. Local circuit neurons in the medial prefrontal cortex (areas 24a, b, c, 25 and 32) in the monkey: II. Quantitative areal and laminar distributions. J Comp Neurol. 1996;364:609-636.

Gallelli CA, et al. Modulation of the oxidative stress and lipid peroxidation by endocannabinoids and their lipid analogues. Antioxidants (Basel). 2018;7:93.

Gamage TF, et al. Synthetic cannabinoid hydroxypentyl metabolites retain efficacy at human cannabinoid receptors. J Pharmacol Exp Ther. 2019;368:414-422.

Garas FN, et al. Structural and molecular heterogeneity of calretinin-expressing interneurons in the rodent and primate striatum. J Comp Neurol. 2018;526:877-898.

Garcia MM et al. Chronic morphine decreases calbindin D28k immunoreactivity in a subset of cerebellar purkinje neurons of rat brain. Brain Res. 1996; 734:123-134.

Gerfen CR, Baimbridge KG, Miller JJ. The neostriatal mosaic: compartmental distribution of calcium-binding protein and parvalbumin in the basal ganglia of the rat and monkey. Proc Natl Acad Sci U S A. 1985;82:8780-8784.

Glass M, Northup JK. Agonist selective regulation of G proteins by cannabinoid CB(1) and CB(2) receptors. Mol Pharmacol. 1999;56:1362-1369.

Gleichmann M, Mattson MP. Neuronal calcium homeostasis and dysregulation. Antioxid Redox Signal. 2011; 14(7):1261-1273.

Grossauer S, et al. Behavioral disorders and cognitive impairment associated with cerebellar lesions. J Mol Psychiatry. 2015;3:5.

Hantman AW, Jessell TM. Clarke's column neurons as the focus of a corticospinal corollary circuit. Nat Neurosci. 2010;13:1233-1239.

Harvey RJ, Napper RM. Quantitative studies of the mammalian cerebellum. Prog Neurobiol. 1991;36:437-463.

Heath RG, Harper JW. Ascending projections of the cerebellar fastigial nucleus to the hippocampus, amygdala, and other temporal lobe sites: evoked potential and histological studies in monkeys and cats. Exp Neurol. 1974;45:268-287.

Heath RG, Harper JW. Ascending projections of the cerebellar fastigial nucleus to the hippocampus, amygdala, and other temporal lobe sites: evoked potential and histological studies in monkeys and cats. Exp Neurol. 1974; 45(2):268-287.

Hebert-Chatelain E et al. A cannabinoid link between mitochondria and memory. Nature. 2016; 539:555–559.

Heck J et al. More than a pore: How voltage-gated calcium channels act on different levels of neuronal communication regulation. Channels (Austin). 2021; 15(1):322-338.

Heizmann CW. Calcium signaling in the brain. Acta Neurobiol Exp (Wars). 1993;53:15-23.

Herculano-Houzel S, Mota B, Lent R. Cellular scaling rules for rodent brains. Proc Natl Acad Sci U S A. 2006;103:12138-12143.

Hermanson DJ et al. Substrate-selective COX-2 inhibition as a novel strategy for therapeutic endocannabinoid augmentation. Trends Pharmacol Sci. 2014; 35(7):358-367.

Himmel NJ, Cox DN. Transient receptor potential channels: Current perspectives on evolution, structure, function and nomenclature. Proc Biol Sci. 2020;287:20201309.

Hoffman AF, Lupica CR. Mechanisms of cannabinoid inhibition of GABA(A) synaptic transmission in the hippocampus. J Neurosci. 2000;20:2470-2479.

Hooks BM, et al. Laminar analysis of excitatory local circuits in vibrissal motor and sensory cortical areas. PLoS Biol. 2011;9:e1000572.

Howlett AC, et al. International Union of Pharmacology. XXVII. Classification of cannabinoid receptors. Pharmacol Rev. 2002;54:161-202.

Howlett AC. Cannabinoid inhibition of adenylate cyclase. Biochemistry of the response in neuroblastoma cell membranes. Mol Pharmacol. 1985;27:429-436.

Howlett AC. Cannabinoid receptor signaling. Handb Exp Pharmacol. 2005;168:53-79.

Huang CC, Lo SW, Hsu KS. Presynaptic mechanisms underlying cannabinoid inhibition of excitatory synaptic transmission in rat striatal neurons. J Physiol. 2001;532:731-748.

Iacopino AM et al. Calcium binding protein (calbindin-D28k) gene expression in the developing and aging mouse cerebellum. Mol Brain Res. 1990; 8:283-290.

Iacopino AM, Christakos S. Specific reduction of calcium-binding protein (28-kilodalton calbindin-D) gene expression in aging and neurodegenerative diseases. Proc Natl Acad Sci U S A. 1990;87:4078-4082.

Iannotti FA, Vitale RM. The endocannabinoid system and PPARs: focus on their signalling crosstalk, action and transcriptional regulation. Cells. 2021; 10:586.

Irie T, et al. MAM-2201, a synthetic cannabinoid drug of abuse, suppresses the synaptic input to cerebellar Purkinje cells via activation of presynaptic CB1 receptors. Neuropharmacology. 2015;95:479-491.

Jacobi H, et al. Update cerebellum and cognition. J Neurol. 2021;268:3921-3925.

Jessen NA, et al. The glymphatic system: a beginner's guide. Neurochem Res. 2015;40:2583-2599.

Jiang X, et al. Principles of connectivity among morphologically defined cell types in adult neocortex. Science. 2015;350:aac9462.

Jin W, et al. Distinct domains of the CB1 cannabinoid receptor mediate desensitization and internalization. J Neurosci. 1999;19:3773-3780.

Jinno S, Kosaka T. Parvalbumin is expressed in glutamatergic and GABAergic corticostriatal pathway in mice. J Comp Neurol. 2004; 477:188–201.

Joseph AM, et al. Characteristics associated with synthetic cannabinoid use among patients treated in a public psychiatric emergency setting. Am J Drug Alcohol Abuse. 2017;43:117-122.

Kano M et al. Endocannabinoid-mediated control of synaptic transmission. Physiol Rev. 2009; 89(1):309-380.

Kawamura Y, et al. The CB1 cannabinoid receptor is the major cannabinoid receptor at excitatory presynaptic sites in the hippocampus and cerebellum. J Neurosci. 2006;26:2991-3001.

Kevin RC, et al. In vitro and in vivo pharmacokinetics and metabolism of synthetic cannabinoids CUMYL-PICA and 5F CUMYL-PICA. Forensic Toxicol. 2017;35:333-347.

Kim BJ et al. Optimized immunohistochemical analysis of cerebellar purkinje cells using a specific biomarker, calbindin d28k. Korean J Physiol Pharmacol. 2009; 13:373–378.

Kim EH, et al. Cortical interneuron loss and symptom heterogeneity in Huntington disease. Ann Neurol. 2014;75:717-727.

Klintworth GK. The comparative anatomy and phylogeny of the tentorium cerebelli. Anat Rec. 1968;160:635-641.

Koob GF, Volkow ND. Neurocircuitry of addiction. Neuropsychopharmacology. 2010;35:217-238.

Koós T, Tepper JM. Inhibitory control of neostriatal projection neurons by GABAergic interneurons. Nat Neurosci. 1999;2:467-472.

Koutsikou S, et al. Neural substrates underlying fear-evoked freezing: the periaqueductal grey-cerebellar link. J Physiol. 2014;592:2197-2213.

Kouznetsova M, et al. Desensitization of cannabinoid-mediated presynaptic inhibition of neurotransmission between rat hippocampal neurons in culture. Mol Pharmacol. 2002;61:477-485.

Kreitzer AC, Malenka RC. Striatal plasticity and basal ganglia circuit function. Neuron. 2008;60:543-554.

Kreitzer AC, Regehr WG. Retrograde inhibition of presynaptic calcium influx by endogenous cannabinoids at excitatory synapses onto Purkinje cells. Neuron. 2001;29:717-727.

Kuczenski R, et al. Escalating dose-multiple binge methamphetamine exposure results in degeneration of the neocortex and limbic system in the rat. Exp Neurol. 2007;207:42-51.

Lauckner JE et al. GPR55 is a cannabinoid receptor that increases intracellular calcium and inhibits M current. Proc Natl Acad Sci U S A. 2008; 105:2699–2704.

Lauckner JE, Hille B, Mackie K. The cannabinoid agonist WIN 55,212-2 increases intracellular calcium via CB1 receptor coupling to Gq/11 G proteins. Proc Natl Acad Sci U S A. 2005;102:19144-19149.

Lee ES, Jeon CJ. Starburst amacrine cells express parvalbumin but not calbindin and calretinin in rabbit retina. Neuroreport. 2013; 24:918–923.

Leo LM, Familusi B, Hoang M, Smith R, Lindenau K, Sporici KT, et al. GPR55-mediated effects on brain microvascular endothelial cells and the blood–brain barrier. Neuroscience. 2019;414:88–98.

Liang YC, et al. Cannabinoid-induced presynaptic inhibition at the primary afferent trigeminal synapse of juvenile rat brain stem slices. J Physiol. 2004;555:85-96.

Liechti ME. Novel psychoactive substances (designer drugs): overview and pharmacology of modulators of monoamine signaling. Swiss Med Wkly. 2015;145:w14043.

Loucif KC, et al. Functional interconnectivity between the globus pallidus and the subthalamic nucleus in the mouse brain slice. J Physiol. 2005;567:977-987.

Lu HC, Mackie K. An introduction to the endogenous cannabinoid system. Biol Psychiatry. 2016; 79(7):516-525.

Luk T et al. Identification of a potent and highly efficacious, yet slowly desensitizing CB1 cannabinoid receptor agonist. Br J Pharmacol. 2004; 142(3):495-500.

Lüscher C, Malenka RC. NMDA receptor-dependent long-term potentiation and long-term depression (LTP/LTD). Cold Spring Harb Perspect Biol. 2012;4:a005710.

Lüscher C, Malenka RC. NMDA receptor-dependent long-term potentiation and long-term depression (LTP/LTD). Cold Spring Harb Perspect Biol. 2012; 4(6):a005710.

Mackie K, et al. Cannabinoids activate an inwardly rectifying potassium conductance and inhibit Q-type calcium currents in AtT20 cells transfected with rat brain cannabinoid receptor. J Neurosci. 1995;15:6552-6561.

Mackie K, Hille B. Cannabinoids inhibit N-type calcium channels in neuroblastoma-glioma cells. Proc Natl Acad Sci U S A. 1992;89:3825-3829.

Mackie K. Distribution of cannabinoid receptors in the central and peripheral nervous system. In: Pertwee RG, editor. Cannabinoids. Berlin, Heidelberg: Springer; 2005. p. 299-325.

Malsam J et al. Membrane traffic in the secretory pathway: membrane fusion: SNAREs and regulation. Cell Mol Life Sci. 2008; 65(18):2814-2832.

Marsicano G, Lutz B. Neuromodulatory functions of the endocannabinoid system. J Endocrinol Invest. 2006; 29(3 Suppl):27-46.

Martini FH, et al. Istologia Testo e Atlante. 2ª ed. Casa Editrice Ambrosiana; 2016.

Martynoga B, Drechsel D, Guillemot F. Molecular control of neurogenesis: a view from the mammalian cerebral cortex. Cold Spring Harb Perspect Biol. 2012;4:a008359.

May B, et al. Synthetic Cannabinoid Receptor Agonists Detection Using Fluorescence Spectral Fingerprinting. Anal Chem. 2019;91:12971-12979.

Miliano C, et al. Neuropharmacology of new psychoactive substances (NPS): focus on the rewarding and reinforcing properties of cannabimimetics and amphetamine-like stimulants. Front Neurosci. 2016;10:153.

Mishra OP, Delivoria-Papadopoulos M. Cellular mechanisms of hypoxic injury in the developing brain. Brain Res Bull. 1999;48(3):233-8.

Mogler L, et al. Phase I metabolism of the carbazole-derived synthetic cannabinoids EG-018, EG-2201, and MDMB-CHMCZCA and detection in human urine samples. Drug Test Anal. 2018;10:1417-1429.

Morales P, Jagerovic N. Advances Towards The Discovery of GPR55 Ligands. Curr Med Chem. 2016; 23:2087–2100.

Moussouttas M. Cannabis use and cerebrovascular disease. Neurologist. 2004;10:47-53.

Muñoz-Castañeda R et al. Cellular anatomy of the mouse primary motor cortex. Nature. 2021; 598(7879):159-166.

Muñoz-Castañeda R, et al. Cellular anatomy of the mouse primary motor cortex. Nature. 2021;598:159-166.

Nagase T, et al. Long-term potentiation and long-term depression in hippocampal CA1 neurons of mice lacking the IP3 type 1 receptor. Neuroscience. 2003;117:821-830.

Neher E, Sakaba T. Multiple roles of calcium ions in the regulation of neurotransmitter release. Neuron. 2008; 59(6):861-872.

Nomura DK et al. Endocannabinoid hydrolysis generates brain prostaglandins that promote neuroinflammation. Science. 2011; 334(6057):809-813.

Nyíri G et al. CB1 cannabinoid receptors are enriched in the perisynaptic annulus and on preterminal segments of hippocampal GABAergic axons. Neuroscience. 2005; 136(3):811-822.

O'Sullivan SE. An update on PPAR activation by cannabinoids. Br J Pharmacol. 2016; 173:1899–1910.

Ossato A, et al. Effect of JWH-250, JWH-073 and their interaction on "tetrad", sensorimotor, neurological and neurochemical responses in mice. Prog Neuropsychopharmacol Biol Psychiatry. 2016;67:31-50.

Ossato A, et al. JWH-018 impairs sensorimotor functions in mice. Neuroscience. 2015;300:174-188.

Ossato A, et al. Psychostimulant Effect of the Synthetic Cannabinoid JWH-018 and AKB48: Behavioral, Neurochemical, and Dopamine Transporter Scan Imaging Studies in Mice. Front Psychiatry. 2017;8:130.

Oztas E et al. Inflammation and oxidative stress are key mediators in AKB48-induced neurotoxicity in vitro. Toxicol In Vitro. 2019; 55:101–107.

Pacher P et al. The endocannabinoid system as an emerging target of pharmacotherapy. Pharmacol Rev. 2006; 58(3):389-462.

Pan WX, Mao T, Dudman JT. Inputs to the dorsal striatum of the mouse reflect the parallel circuit architecture of the forebrain. Front Neuroanat. 2010;4:147.

Park D, et al. Prominent astrocytic GLAST pathology occurs in newborn human and piglet hypoxic-ischemic encephalopathy: modeling relationships among laminar neuropathology, seizures, and therapeutic hypothermia. Front Cell Neurosci. 2026;20:1758411.

Patel S, Hillard CJ. Cannabinoid CB1 receptor agonists produce cerebellar dysfunction in mice. J Pharmacol Exp Ther. 2001;297:629-637.

Paxinos G, editor. The rat nervous system. 4th ed. San Diego: Academic Press; 2014.

Permyakov EA, Uversky VN. What is parvalbumin for? Biomolecules. 2022;12:656.

Pertwee RG, et al. International Union of Basic and Clinical Pharmacology. LXXIX. Cannabinoid receptors and their ligands: beyond CB1 and CB2. Pharmacol Rev. 2010;62:588-631.

Pertwee RG. Cannabinoid receptor ligands: clinical and neuropharmacological considerations, relevant to future drug discovery and development. Expert Opin Investig Drugs. 2000;9:1553-1571.

Petersen CC. The functional organization of the barrel cortex. Neuron. 2007;56:339-355.

Petryszyn S, et al. A dense cluster of D1+ cells in the mouse nucleus accumbens. Synapse. 2017;71:51-54.

Pickel VM, Heras A. Ultrastructural localization of calbindin-D28k and GABA in the matrix compartment of the rat caudate-putamen nuclei. Neuroscience. 1996;71:167-178.

Pikor D, et al. Calcium Ions in the Physiology and Pathology of the Central Nervous System. Int J Mol Sci. 2024;25:13133.

Planert H, Berger TK, Silberberg G. Membrane properties of striatal direct and indirect pathway neurons in mouse and rat slices and their modulation by dopamine. PLoS One. 2013;8:e57054.

Reiner A, et al. Striatal parvalbuminergic neurons are lost in Huntington's disease: implications for dystonia. Mov Disord. 2013;28:1691-1699.

Résibois A, Rogers JH. Calretinin in rat brain: An immunohistochemical study. Neuroscience. 1992; 46:101–134.

Rogers JH. Calretinin: a gene for a novel calcium-binding protein expressed principally in neurons. J Cell Biol. 1987;105:1343-1353.

Roque-Bravo R, et al. Synthetic cannabinoids: a pharmacological and toxicological overview. Annu Rev Pharmacol Toxicol. 2023;63:187-209.

Rubino T, et al. Chronic CP-55,940 alters cannabinoid receptor mRNA in the rat brain: an in situ hybridization study. Neuroreport. 1994;5:2493-2496.

Ruden JB, Dugan LL, Konradi C. Parvalbumin interneuron vulnerability and brain disorders. Neuropsychopharmacology. 2021;46:279-287.

Santos Ferreira C. Staining of intestinal protozoa with Heidenhain's iron hematoxylin. Rev Inst Med Trop Sao Paulo. 2003;45:43-44.

Sato M et al. Histological changes of neuronal damage in vegetative dogs induced by 18 minutes of complete global brain ischemia: Two phase damage of purkinje cells and hippocampal CA1 pyramidal cells. Acta Neuropathol (Berl). 1990; 80:527-534.

Schilling K, et al. Besides Purkinje cells and granule neurons: an appraisal of the cell biology of the interneurons of the cerebellar cortex. Histochem Cell Biol. 2008;130:601-615.

Schröder H, Moser N, Huggenberger S. Neuroanatomy of the mouse: An introduction. Cham: Springer Nature, 2020

Schwaller B. Calretinin: from a “simple” Ca2+ buffer to a multifunctional protein implicated in many biological processes. Front Neuroanat. 2014;8:3.

Schwaller B. Cytosolic Ca2+ buffers. Cold Spring Harb Perspect Biol. 2010;2:a004051.

Seibert MJ et al. Synaptotagmin 9 modulates spontaneous neurotransmitter release in striatal neurons by regulating substance P secretion. J Neurosci. 2023; 43(9):1475-1491.

Sezer Y et al. In vitro assessment of the cytotoxic, genotoxic and oxidative stress effects of the synthetic cannabinoid JWH-018 in human SH-SY5Y neuronal cells. Toxicol Res (Camb). 2020; 9:734–740.

Shafi A, et al. New psychoactive substances: a review and updates. Ther Adv Psychopharmacol. 2020;10:2045125320967197.

Siesjo BK et al. Is the cell death pathway triggered by the mitochondrion or the endoplasmic reticulum? J Cereb Blood Flow Metab. 1999; 19:19-26.

Simão AY, et al. An Update on the Implications of New Psychoactive Substances in Public Health. Int J Environ Res Public Health. 2022;19:4869.

Simon G et al. Fatal Overdose with the Cannabinoid Receptor Agonists MDMB-4en-PINACA and 4F-ABUTINACA: A Case Report and Review of the Literature. Toxics. 2023; 11:673.

Simons M, Nave KA. Oligodendrocytes: myelination and axonal support. Cold Spring Harb Perspect Biol. 2016;8:a020479.

Sim-Selley LJ. Regulation of cannabinoid CB1 receptors in the central nervous system by chronic cannabinoids. Crit Rev Neurobiol. 2003;15:91-119.

Sobolevsky T, Prasolov I, Rodchenkov G. Detection of JWH-018 metabolites in smoking mixture post-administration urine. Forensic Sci Int. 2010;200:141-147.

Stevens FC. Calmodulin: An introduction. Can J Biochem Cell Biol. 1983;61:906-910.

Stichel CC, et al. Immunohistochemical localization of calcium-binding proteins, parvalbumin and calbindin-D 28k, in the adult and developing visual cortex of cats: A light and electron microscopic study. J Comp Neurol. 1987;262:563-577.

Strange BA, et al. Functional organization of the hippocampal longitudinal axis. Nat Rev Neurosci. 2014;15:655-669.

Sullivan JM. Mechanisms of cannabinoid-receptor-mediated inhibition of synaptic transmission in cultured hippocampal pyramidal neurons. J Neurophysiol. 1999;82:1286-1294.

Sun T, Hevner R. Growth and folding of the mammalian cerebral cortex: from molecules to malformations. Nat Rev Neurosci. 2014;15:217-232.

Sun XZ, et al. Distribution of calbindin-D28K immunoreactive neurons in rat primary motor cortex. J Med Invest. 2002;49:35-39.

Takagi M, Zee DS, Tamargo RJ. Effects of lesions of the oculomotor cerebellar vermis on eye movements in primate: smooth pursuit. J Neurophysiol. 2000;83:2047-2062.

Takayama T, et al. UPLC/ESI-MS/MS-based determination of metabolism of several new illicit drugs, ADB-FUBINACA, AB-FUBINACA, AB-PINACA, QUPIC, 5F-QUPIC and α-PVT, by human liver microsome. Biomed Chromatogr. 2014;28:831-838.

Talamoni N et al. Immunocytochemical localization of the plasma membrane calcium pump, calbindin-D28k, and parvalbumin in purkinje cells of avian and mammalian cerebellum. Proc Natl Acad Sci U S A. 1993; 90:11949-11953

Tauskela JS, et al. Effect of synthetic cannabinoids on spontaneous neuronal activity: Evaluation using Ca(2+) spiking and multi-electrode arrays. Eur J Pharmacol. 2016;786:148-160.

Tepper JM, et al. Heterogeneity and diversity of striatal GABAergic interneurons. Front Neuroanat. 2010;4:150.

Tepper JM, Koós T, Wilson CJ. GABAergic microcircuits in the neostriatum. Trends Neurosci. 2004;27:662-669.

Tlamsa AP, Brumberg JC. Organization and morphology of thalamocortical neurons of mouse ventral lateral thalamus. Somatosens Mot Res. 2010;27:34-43.

Tomiyama K, Funada M. Cytotoxicity of synthetic cannabinoids on primary neuronal cells of the forebrain: the involvement of cannabinoid CB1 receptors and apoptotic cell death. Toxicol Appl Pharmacol. 2014;274:17-23.

Tomiyama M et al. Flip and flop variants of AMPA receptor subunits in the human cerebellum: Implication for the selective vulnerability of purkinje cells. Synapse. 1999; 31:163-167.

Tremblay R, Lee S, Rudy B. GABAergic interneurons in the neocortex: from cellular properties to circuits. Neuron. 2016;91:260-292.

Treuting PM, et al., editors. Comparative Anatomy and Histology: A Mouse and Human Atlas. Academic Press; 2012.

Uchiyama N, et al. Identification of two new-type synthetic cannabinoids, N-(1-adamantyl)-1-pentyl-1H-indole-3-carboxamide (APICA) and N-(1-adamantyl)-1-pentyl-1H-indazole-3-carboxamide (APINACA), and detection of five synthetic cannabinoids, AM-1220, AM-2233, AM-

1241, CB-13 (CRA-13), and AM-1248, as designer drugs in illegal products. Forensic Toxicol. 2012;30:114-125.

Utz A, et al. Cerebellar vermis contributes to the extinction of conditioned fear. Neurosci Lett. 2015;604:173-177.

van Amsterdam J et al. The adverse health effects of synthetic cannabinoids with emphasis on psychosis-like effects. J Psychopharmacol. 2015; 29(3):254-263.

Van Brederode JF et al. Distribution of the calcium-binding proteins parvalbumin and calbindin-D28k in the sensorimotor cortex of the rat. Neuroscience. 1991; 44:157–171.

Van Sickle MD, et al. Identification and functional characterization of brainstem cannabinoid CB2 receptors. Science. 2005;310:329-332.

Vardakou I, Pistos C, Spiliopoulou Ch. Spice drugs as a new trend: Mode of action, identification and legislation. Toxicol Lett. 2010;197:157-162.

Vigolo A, et al. Novel halogenated derivates of JWH-018: Behavioral and binding studies in mice. Neuropharmacology. 2015;95:68-82.

Volpe P et al. Multiple/heterogeneous Ca2+ stores in cerebellum purkinje neurons. Comp Biochem Physiol Comp Physiol. 1993; 105:205-211.

Walsh KB, Andersen HK. Molecular pharmacology of synthetic cannabinoids: delineating CB1 receptor-mediated cell signaling. Int J Mol Sci. 2020; 21(17):6115.

Wayman GA, et al. Calmodulin-kinases: modulators of neuronal development and plasticity. Neuron. 2008;59:914-931.

White JJ, Sillitoe RV. Development of the cerebellum: from gene expression patterns to circuit maps. Wiley Interdiscip Rev Dev Biol. 2013;2:149-164.

White JJ, Sillitoe RV. Development of the cerebellum: from gene expression patterns to circuit maps. Wiley Interdiscip Rev Dev Biol. 2013; 2(1):149-164.

Wohlfarth A, et al. Urinary prevalence, metabolite detection rates, temporal patterns and evaluation of suitable LC-MS/MS targets to document synthetic cannabinoid intake in US military urine specimens. Clin Chem Lab Med. 2015;53:423-434.

Woodward DF et al. The pharmacology and therapeutic relevance of endocannabinoid derived cyclo-oxygenase (COX)-2 products. Pharmacol Ther. 2008; 120(1):71-80.

Wree A et al., A quantitative approach to cytoarchitectonics: VIII. The areal pattern of the cortex of the albino mouse. Anat Embryol (Berl). 1983;166:333-353.

Xiao L, Scheiffele P. Local and long-range circuit elements for cerebellar function. Curr Opin Neurobiol. 2018;48:146-152.

Xiao L, Scheiffele P. Local and long-range circuit elements for cerebellar function. Curr Opin Neurobiol. 2018; 48:146-152.

Yáñez M et al. Calcium binding proteins. In: Islam MS, editor. Calcium Signaling. Dordrecht: Springer; 2012. p. 461-482.

Yáñez M et al., Calcium binding proteins. In: Islam MS, editor. Calcium Signaling. Springer; 2012. p. 461-482.

Yi CW et al. Types of parvalbumin-containing retinotectal ganglion cells in mouse. Acta Histochem Cytochem. 2012; 45:201–210.

Zanelli SA et al. NMDA receptor-mediated calcium influx in cerebral cortical synaptosomes of the hypoxic guinea pig fetus. Neurochem Res. 1999; 24:437-446.

Zeiss CJ. Neuroanatomical phenotyping in the mouse: the dopaminergic system. Vet Pathol. 2005;42:753-773.

Zhang Q, et al. Identification of in vitro metabolites of JWH-015, an aminoalkylindole agonist for the peripheral cannabinoid receptor (CB2) by HPLC-MS/MS. Anal Bioanal Chem. 2006;386:1345-1355.

Zhuang SY, et al. Effects of long-term exposure to Δ9-THC on expression of cannabinoid receptor (CB1) mRNA in different rat brain regions. Brain Res Mol Brain Res. 1998;62:141-149.

Websites

https://www.euda.europa.eu/topics/pods/synthetic-cannabinoids_en